A Section 508–conformant HTML version of this article is available at https://doi.org/10.1289/EHP7349.

Characterizing the Low-Dose Effects of Methylmercury on the Early Stages of Embryo Development Using Cultured Human Embryonic Stem Cells

Bai Li,[1] Cunye Qiao,[2] Xiaolei Jin,[3] and Hing Man Chan[1]

[1]Department of Biology, University of Ottawa, Ottawa, Ontario, Canada
[2]Biostatistics and Modeling Division, Bureau of Food Surveillance and Science Integration, Food Directorate, Health Products and Food Branch (HPFB), Health Canada, Ottawa, Ontario, Canada
[3]Regulatory Toxicology Research Division, Bureau of Chemical Safety, Food Directorate, HPFB, Health Canada, Ottawa, Ontario, Canada

Background: Global concerns of methylmercury (MeHg) exposure have been raised, especially on its effects on pregnant women. Recent epidemiological studies have revealed associations between maternal blood/hair MeHg concentrations, adverse pregnancy outcomes, and developmental deficits. However, the underlying mechanisms remain unclear.

Objectives: In this study, we characterized the effects of MeHg exposure on undifferentiated human embryonic stem cells (hESCs) and extrapolated the effects to human embryonic development.

Methods: hESCs were exposed to 0, 1, 5, 10, 50, 100 or 200 nM MeHg for 24 h or 6 d. Cell adherence and colony formation and expansion were examined under the microscope. Cell attachment, viability/proliferation, apoptosis, stress response, cell cycle, autophagy, and expression of cell lineage marker genes and proteins were measured at the end of exposures.

Results: Our results indicated that exposure to nanomolar concentrations of MeHg was associated with *a*) higher levels of reactive oxygen species (ROS) and hemeoxygenase-1 (HO-1), suggesting increased stress and adaptive responses; *b*) lower cellular adhesion, viability/proliferation, and colony formation and expansion; *c*) higher levels of apoptosis, reflected by higher cleaved caspase-3 expression and Annexin V binding; *d*) higher levels of cytoskeleton protein α-tubulin expression; *e*) higher rates of G1/S phase cell cycle arrest; and *f*) autophagy inhibition, as shown by a lower LC3BII/LC3BI ratio and accumulation of SQSTM1 (p62). These outcomes were accompanied by higher expressions of self-renewal genes or proteins or both, including OCT4, SOX2, NANOG, and cytokine receptor IL6ST, as well as pluripotency and the cell fate regulator cyclin D1.

Discussion: These results revealed that under the selection pressure of exposure to low doses of MeHg, some hESCs underwent apoptosis, whereas others adapted and survived with enhanced self-renewal gene expression and specific morphological phenotypes. Findings from the present study provide *in vitro* evidence that low doses of MeHg adversely affect hESCs when exposed during a period of time that models embryonic pre-, during, and early postimplantation stages. https://doi.org/10.1289/EHP7349

Introduction

It is increasingly recognized that early embryonic development is susceptible to environmental stressors, such as chemical contaminants. Exposure to chemicals can alter cellular programming and differentiation, not only shaping the phenotype of health and disease later in life but also influencing the vulnerability of subsequent generations (Hanson and Skinner 2016; Heindel 2019). Therefore, understanding the effects of chemical exposure at early developmental stages is essential for the assessment and mitigation of the health risks associated with prenatal chemical exposure. Mercury is a ubiquitous environmental contaminant (Driscoll et al. 2013). Humans are exposed to mercury as methylmercury (MeHg) mainly through fish and marine mammal consumption (Canuel et al. 2006; Chan and Receveur 2000; Mahaffey et al. 2011). Once consumed, MeHg forms a complex with cysteine and homocysteine and is transported by amino acid transporters across the blood–brain barrier and the placenta and throughout the body (Kerper et al. 1992).

Most studies on the developmental toxicity of mercury have focused on its neurological effects (Ceccatelli et al. 2010; dos Santos et al. 2016; Grandjean and Herz 2011; Shao et al. 2015; Sheehan et al. 2014). Several studies have shown that mammalian neuroprogenitor cells (NPCs) are highly sensitive to MeHg, which induce apoptosis at nanomolar concentrations (Edoff et al. 2017; Tamm et al. 2006; Watanabe et al. 2013). Birth cohort studies on populations of the Faroe Islands have revealed associations between cognitive deficits and prenatal MeHg exposure predominantly via the consumption of marine mammals (pilot whale meat), which remained detectable at 7 (Grandjean et al. 1997), 14 (Debes et al. 2006), and 22 years of age (Debes et al. 2006, 2016; Grandjean et al. 1997). Prenatal exposure to mercury has been reported to be associated with neurodevelopmental deficits in motor skill, attention (Debes et al. 2006), language skill, memory function (Choi et al. 2014), visual function (Karagas et al. 2012), and general intelligence (Debes et al. 2016) in infants (Oken et al. 2005), children (Prpić et al. 2017), and youth (Choi et al. 2014; Debes et al. 2006, 2016; Ha et al. 2017; Julvez et al. 2010; Karagas et al. 2012; Oken et al. 2005; Prpić et al. 2017). However, the effects of prenatal exposure to MeHg on the development of other organs and systems remain uncertain (Karagas et al. 2012).

Human embryonic stem cells (hESCs) are undifferentiated immature cells with the capacity of self renewal and the potential to differentiate into all specific cell types in the human body (Thomson et al. 1998). The majority of primary hESC lines were separated from the inner cell mass (ICM) of blastocysts cultured from cleavage-stage human embryos that were generated from *in vitro* fertilization for clinical purposes (Thomson et al. 1998). The health and fate of hESCs determine their capability and the potential to proliferate or differentiate into endoderm, ectoderm, and mesoderm lineage cells. Each of these lineages then further

Address correspondence to Xiaolei Jin, Regulatory Toxicology Research Division, Bureau of Chemical Safety, Food Directorate, Health Products and Food Branch, Health Canada, 251 Sir Frederick Banting Driveway, Ottawa, Ontario, Canada K1A 0K9. Email: dawn.jin@canada.ca, or Hing Man Chan, Department of Biology, University of Ottawa, 30 Marie Curie, Ottawa, Ontario Canada K1N 6N5. Email: laurie.chan@uottawa.ca

Supplemental Material is available online (https://doi.org/10.1289/EHP7349).

The authors declare they have no actual or potential competing financial interests.

Received 30 April 2020; Revised 18 June 2021; Accepted 2 July 2021; Published 30 July 2021.

differentiates into cells of different organs and systems; examples of this differentiation include the endoderm forming gut epithelial cells, pancreas, and hepatocytes; the ectoderm forming neural epithelium, embryonic ganglia, and stratified squamous epithelium; and the mesoderm forming cartilage, bone, and smooth and striated muscles (Li et al. 2015; Thomson et al. 1998). Genetic or epigenetic alterations in hESCs induced by environmental stressors, if they occur *in vivo*, may affect the fate and development of the embryo and the health status of the individual later in life (Worley and Parker 2019). MeHg exposures have been associated with a higher number of abnormal blastocysts (Kajiwara and Inouye 1986) and blastocyst degeneration (Spindle and Matsumoto 1987) in mice. However, there is a lack of in-depth studies of the effects of MeHg on early embryo developmental processes, such as during the blastocyst stage, which spans from Day 5 to Day 12 after fertilization (Lopata 1996).

Therefore, the main objective of the present study was to investigate the effects of MeHg in hESCs as a model to extrapolate to human embryonic development. We hypothesized that exposure of hESCs to low concentrations of MeHg might affect the fate and health status of blastocysts, which, if it occurs *in vivo*, would disrupt early embryo development and result in adverse pregnancy outcomes. To test this hypothesis, we examined the impact of MeHg on a number of parameters, including colony formation, viability/proliferation, apoptosis, stress response, cell cycle, autophagy, cytoskeleton protein expression, and cell lineage marker gene and protein expression in hESCs under culture conditions for 24 h or 6 d of MeHg exposure, modeling the *in vivo* acute exposure and continuous exposure of MeHg throughout the pre-, during, and early postimplantation stages.

Materials and Methods

Ethics Review and Approval

This project was reviewed and approved by the Health Canada and Public Health Agency of Canada's Research Ethics Board (File No. REB 2016-027H) and by the Office of Research Ethics and Integrity of the University of Ottawa (File No. H-05-19-4084).

Cell Maintenance and Expansion

Human embryonic stem cells (H9; passage 23) were purchased from WiCell Research Institute and adapted and expanded in Matrigel (Catalog no. 354 230; BD Biosciences) precoated six-well plates containing Essential 8 Flex Medium (Catalog no. A2858501; Thermo Fisher Scientific) under 37°C, 4% oxygen (O_2) and 10% carbon dioxide (CO_2) in a tri-gas incubator (Thermo Fisher Scientific). Culture conditions were optimized to allow high viability and attachment upon plating and maintain pluripotency without any visible differentiation during 7 d of culturing (Figure S1). Ten-micromolar Rho-associated kinase inhibitor (Catalog no. 72304; StemCell Technologies) was added to the medium, which was changed daily. For passaging, cells were lifted using Gibco Versene Solution (Catalog no. 15040066; Thermo Fisher Scientific). Cells at 85% confluence were either frozen in mFreSR cryopreservation medium (Catalog no. 05855; StemCell Technologies) or used for dosing experiments. To avoid the genetic instability associated with prolonged passaging, only the hESCs under passage 38 (within 15 passages from purchase) were used.

On the seventh day of continuous culture, the expression of pluripotency markers, octamer-binding transcription factor 4 [OCT4; also known as POU5F1 (POU domain, class 5, transcription factor 1)] and the Tra-1-81 antibody were determined by immunocytochemical staining (Figure S2). Briefly, the medium was disposed and the cells were washed twice with phosphate-buffered saline (PBS), fixed in 4% paraformaldehyde (Santa Cruz Biotechnology) for 10 min, and then blocked with 5% bovine serum albumin (BSA) diluted in PBS containing 0.3% Triton X-100 (Sigma-Aldrich). The cells were then incubated with rabbit antihuman OCT4 antibody (Catalog no. C30A3; Cell Signaling Technology) and mouse antihuman Tra-1-81 antibody (Catalog no. 4745; Cell Signaling Technology) diluted at 1:200 in 5% BSA in PBS, at 4°C overnight. After washing three times with PBS, the cells were incubated with Alexa Fluor 488 goat antirabbit immunoglobulin G (IgG) (Catalog no. A11008; Thermo Fisher Scientific) and Alexa Fluor 594 goat antimouse IgG (Catalog no. A11005; Thermo Fisher Scientific) diluted at 1:500 in 5% BSA in PBS at room temperature for 1 h. After washing three times with PBS, the Prolong Gold antifade reagent containing 4′,6-diamidino-2-phenylindole (DAPI; Catalog no. S36939; Thermo Fisher Scientific) was added. The immunofluorescent images were acquired on a Zeiss LSM 880 confocal microscope (Carl Zeiss Canada Ltd.) with Zeiss Efficient Navigation imaging software (version 14.0.21.201).

Chemical Preparation and Exposure

MeHg chloride (purity: 99.9%) was obtained from Sigma-Aldrich and dissolved in 5 mM sodium carbonate (Na_2CO_3) to obtain 100× stock solutions (i.e., 0.1, 0.5, 1, 5, 10, 20, and 50 μM). The hESCs were seeded in 6- or 24-well culture dishes at a density of 1×10^4 cells/mL and allowed to attach for 24 h. Then the cells were exposed to 0 (0.05 mM Na_2CO_3 as vehicle control), 1, 5, 10, 50, 100, 200, or 500 nM MeHg by 100× dilution of the stock solutions in culture dishes, which were incubated at 37°C, 4% O_2, and 10% CO_2 for 24 h or 6 d, with a daily change of medium and dosing to mimic acute exposure and continuous exposure of MeHg throughout the *in vivo* pre-, during, and early postimplantation processes. The measurements of all end points were repeated at least three times, using samples from at least three different passages. Depending on the end points, one or two technical replicates were used.

Cell Attachment and Colony Formation

hESCs were treated with MeHg for 6 d, as described above. Vehicle- and MeHg-treated hESCs were observed and imaged daily under a 10× objective on a Zeiss Axiovert 40 CFL inverted microscope (Carl Zeiss Microscopy LLC) with a SPOT RT3 digital camera and SPOT basic software (Diagnostic Instruments Inc.).

Cell Viability and Proliferation

hESCs were exposed to MeHg in 24-well plates for 6 d, as described above. Tetrazolium salt (WST-1) assays were performed to determine the effects of MeHg on cell viability and proliferation using a WST-1 assay kit (Catalog no. ab155902; Abcam Inc.) according to the manufacturer's instructions. The WST-1 assay measures the cleavage of WST-1 to formazan by cellular mitochondrial dehydrogenases. A greater amount of formazan dye indicates a greater amount or higher activity of cellular mitochondrial dehydrogenases, indicating higher cell numbers or viability. Briefly, 20 μL of WST-1 solution per well was added into the culture in the 24-well plates, followed by shaking for 10 s. Absorbance at 420–480 nm wavelength was measured on a BioTek Cytation 3 Cell Imaging Multi-Mode Reader (Fisher Scientific) after a 1.5-h incubation at 37°C.

Intracellular Total Mercury Content

Intracellular mercury content was measured after 24 h and 6 d of exposure. At the corresponding time points, the culture medium

was first collected. Cells were rinsed twice with 500 μL PBS each time, and the PBS was collected after both rinses. The cells were then collected using a scraper and suspended in 140 μL (for cells after 24 h of MeHg exposure) and 500 μL (for cells after 6 d of MeHg exposure) of clean PBS. Ten microliters of cell suspension was taken from each sample, and cell densities were counted using a Countess Automated Cell Counter (Invitrogen, Thermo Fisher Scientific) after 1:1 dilution of cell suspension in Trypan blue solution (Catalog no. T10282; ThermoFisher Scientific). Total mercury contents in the medium, PBS, and cells were measured using a mercury analyzer (MA 3000; Nippon Instruments Corp.), according to the manufacturer's instructions. Intracellular total mercury was normalized to cell number and reported as picomoles per 10,000 cells.

The end points, apoptosis, cytoskeleton protein expression, stress response, cell cycle, autophagy, cell lineage gene and protein expression were measured in 0, 10, 50, or 200 nM MeHg-treatment groups. Colony formation and expansion, cell viability and proliferation, cellular and medium total mercury concentration, ROS, and Cyclin D1 protein expression were measured in 0, 5, 10, 50, 100, and 200 nM MeHg-treatment groups.

Cell Apoptosis

The Annexin V–fluorescein-5-isothiocyanate (FITC) Early Apoptosis Detection Kit (Catalog no. 6592S; Cell Signaling Technology) was used according to the manufacturer's instructions to detect the effects of MeHg on early apoptosis. Briefly, hESCs were exposed to MeHg as described above for 24 h or 6 d. Cells were detached using Accutase (Catalog no. A11105-01; Thermo Fisher Scientific), resuspended in Annexin V binding buffer, and aliquoted at 96 μL/tube. Then, 1 μL of Annexin V conjugate and 12.5 μL of propidium iodide (PI) were added to each tube and incubated in the dark for 10 min. The cell suspension was then diluted to a final volume of 250 μL using Annexin V binding buffer before analysis. All the steps were conducted on ice. The fluorescent labeling of apoptotic cells was counted on a BD LSR II Flow Cytometer (Becton Dickinson) using 505LP (long pass), 525/50BP (band pass) on the blue (488-nm) laser for detection of the early apoptosis marker Annexin V, whereas 570LP, 582/15BP on the yellow/green (561nm) laser allowed detection of the necrosis marker (i.e., PI). The detached cells were collected by centrifuging the supernatant and subsequently stained with Trypan blue. The cell number was then counted with a Countess Automated Cell Counter.

After hESCs were exposed to MeHg in Matrigel-precoated chamber slides (Catalog no. 0030742010; Eppendorf) for 24 h, the effects of MeHg on intermediate and late apoptosis was determined by measuring the expression of cleaved caspase-3 (CC3), which is an active form of caspase 3 (Konstantinidou et al. 2007), with immunocytochemical staining, as previously described using rabbit antihuman CC3 antibody (Catalog no. 9661S; Cell Signaling Technology) at 1: 200 dilution. The immunofluorescent images were taken with a Nikon A1RsiMP confocal microscope (Nikon Instruments Inc.) with Nikon's Imaging Software NIS-Elements. CC3-positive cells were counted using ImageJ (Hartig 2013), and the percentage of CC3-positive cells was calculated against total counts (DAPI-stained). A higher percentage of CC3-positive cells indicates a higher level of apoptosis. The expression of CC3 of hESCs after 6 d of MeHg exposure was measured by western blot. Briefly, after exposure of hESCs to MeHg in six-well plates for 6 d, the medium was removed, cells were washed with PBS, lysed in Pierce radioimmunoprecipitation assay buffer (RIPA buffer; Thermo Fisher Scientific) containing the proteinase and phosphatase inhibitor cocktails (Catalog no. 5872S; Cell Signaling Technology) on ice, and homogenized by sonication using a Microson Ultrasonic Cell Disruptor XL2000 (Misonix Inc.). The protein concentrations of the lysates were quantified using a Pierce Bicinchoninic Acid Protein Assay kit (Thermo Fisher Scientific). Cell lysates were mixed with 4× Laemmli sample buffer (Bio-Rad) and denatured by heating at 100°C for 4 min. Cell lysates were separated on a Stain-Free gel made with TGX Stain-Free FastCast acrylamide solutions (Catalog no. 161-0185; Bio-Rad). For each batch, the same amount of protein was loaded, and the amount of total protein loaded ranged from 25 to 30 μg between different batches. After electrophoresis, gels were activated under ultraviolet light using the ChemiDoc XRS+ imaging system (Bio-Rad). Proteins were electro-transferred from gels to polyvinylidene difluoride (PVDF) membranes with the Mini Trans-Blot Cell (Catalog no. 1703930; Bio-Rad). Membranes were then blocked with 5% nonfat dry milk (NFDM, Catalog no. 1706404; Bio-Rad) for 1 h at room temperature and incubated with rabbit antihuman CC3 antibody (Catalog no. 9661S; Cell Signaling Technology) (1:1,000 diluted in blocking buffer) at 4°C overnight. After the membranes were washed three times in Tris-buffered saline with 0.1% Tween 20 (TBST) on a shaker for 5 min, they were incubated with horseradish peroxidase (HRP)–linked goat antirabbit secondary antibody (G-21234; Thermo Fisher Scientific) for 1 h at room temperature. All membranes were then incubated with the enhanced chemiluminescence substrate (Catalog no. 1705062; Bio-Rad) in the dark and imaged using the ChemiDoc XRS+ imaging system. The band intensity was quantified and normalized against total protein band intensity using Image Lab software (Bio-Rad). Given that our previous observation suggested that MeHg treatment can influence the expression of some loading control proteins, we used Stain-Free gels in all western blot assays to obtain total protein bands for normalization of target proteins. All secondary antibodies used in western blots were diluted at 1:5,000 in the corresponding blocking buffer.

Cytoskeleton Protein Expression

To determine the effects of MeHg on cytoskeleton protein expression, we used western blots to examine β-actin and α-tubulin expression. The protein extracts were obtained and electrophoresis was conducted as described above after culture and exposure of MeHg for 6 d. Proteins were electro-transferred from gels to PVDF membranes with the Trans-Blot Turbo Transfer System (Bio-Rad). Membranes were then blocked with 3% BSA for 1 h at room temperature and incubated with mouse antihuman α-tubulin antibody (Catalog no. ab4074) (1:1,000 in 3% BSA) and rabbit antihuman β-actin antibody (Catalog no. ab8227; Abcam Inc.) (1:1,000 in 3% BSA) at 4°C overnight. After the membranes were washed three times in TBST on a shaker for 5 min, they were incubated with HRP-linked goat antimouse (Catalog no. P0447; Dako) or HRP-linked goat antirabbit secondary antibody (Catalog no. A16110; Thermo Fisher Scientific) for 1 h at room temperature.

Cellular Stress Response

To quantify MeHg-induced stress and adaptive responses in hESCs, we measured the production of ROS and protein expression of hemeoxygenase-1 (HO-1). To determine the ROS production, CellROX deep red reagent (Catalog no. C10422; Thermo Fisher Scientific) was added into the culture at a final concentration of 5 μM and incubated for 30 min at 37°C. After removing the medium, the cells were washed three times in PBS for 5 min, and the nuclei were stained with DAPI. Images were viewed and acquired using a Zeiss Axiovert 40 CFL inverted microscope (Carl Zeiss Microscopy LLC) with a SPOT RT3 digital camera and SPOT basic software (Diagnostic Instruments Inc.) and

quantified using ImageJ (Hartig 2013). To quantify HO-1 protein expression, we conducted western blot assays, as described above, using antihuman HO-1 as the primary antibody (Catalog no. ab13248; Abcam Inc.) (1:1,000 3% BSA).

Cell Cycle

To determine whether MeHg affects the cell cycle, we examined cyclin A2, cyclin D1, and cyclin E1 protein expression and measured cell cycle phases. hESCs were exposed to MeHg for 6 d, and protein extracts were obtained as described above. Western blot analysis was performed as above using antibodies against human cyclin A2 (Catalog no. ab181591) (1:1,000 in 3% BSA), cyclin D1 (Catalog no. ab134175) (1:1,000 in 3% BSA), and cyclin E1 (Catalog no. ab133266; Abcam Inc.) (1:1,000 in 3% BSA) and goat antirabbit secondary antibody (G-21234; Thermo Fisher Scientific; 1:5,000). Band intensities were quantified and normalized as described above.

For cell cycle assays, hESCs were exposed to MeHg for 6 d, washed with cold PBS, detached by Accutase, centrifuged, and resuspended and stained in the nuclear green CCS1 solution provided in the Cell Cycle Assay kit (Catalog no. ab112116; Abcam Inc.). After incubating for 40 min at 37°C, fluorescent intensity was quantified using a BD LSR II Flow Cytometer (Becton Dickinson) with 505LP, 525/50BP on the blue (488-nm) laser.

Cellular Autophagy

To determine the effects of MeHg on autophagy, we measured the protein expression of microtubule-associated proteins 1A/1B light chain 3B (LC3BI), LC3BII, and sequestosome 1 [SQSTM1 (p62)] using western blots. Once hESCs were exposed to MeHg for 6 d, the cells were lysed in Pierce RIPA buffer containing the proteinase and phosphatase inhibitor cocktails (Catalog no. 5872S; Cell Signaling Technology) on ice, and the cell lysates were collected and measured for total protein and protein LC3BI, LC3BII, and SQSTM1 (p62) using western blots with 4–20% MP TGX Stain-Free gels (Catalog no. 4568094; Bio-Rad) and the Stain-Free technique, as described above. The membranes were immunoblotted with rabbit polyclonal antihuman LC3B antibody (Catalog no. 2775) (1:1,000 in 5% NFDM) from Cell Signaling Technology or mouse monoclonal antihuman p62 antibody (Cat. # ab56416) (1:1,000 in 5% NFDM) from Abcam. Band intensities were quantified as described above.

Cell Lineage Marker Gene Expression

The TaqMan hPSC Scorecard Assay (Catalog no. A15871; Thermo Fisher Scientific) was used to determine the effects of MeHg on cell lineage marker gene expression. hESCs were exposed to MeHg in six-well dishes for 6 d as described above. To isolate total RNA, the cells were washed with PBS and lysed in 1 mL of Invitrogen TRIzol (Thermo Fisher Scientific) for 5 min. The cell lysates were pipetted up and down several times, mixed with 200 μL chloroform (Sigma-Aldrich Canada Ltd.), hand-shaken vigorously, and incubated for 3 min. Supernatants were transferred to new tubes after centrifugation at 4°C and $12,000 \times g$ for 15 min. Isopropanol (0.5 mL/tube) was added, mixed well, and incubated for 10 min. Supernatants were removed after centrifugation at 4°C and $12,000 \times g$ for 10 min. The isolated total RNA was washed with 75% diethylpyrocarbonate-treated ethanol, air-dried, and dissolved in Ambion RNase-free water (Thermo Fisher Scientific). The concentration and quality of RNA were measured using a NanoDrop 1000 (Thermo Fisher Scientific). RNA samples were purified using the Ambion DNA-free kit (Life Technology, Thermo Fisher Scientific). Then, RNA samples were reverse-transcribed with the Applied Biosciences High-Capacity complementary DNA Reverse Transcription kit with RNase inhibitor (Thermo Fisher Scientific), following the manufacturer's instructions. Briefly, RNA samples were mixed with the master mix solution and aliquoted into eight-strip polymerases chain reaction (PCR) tubes. Then the real-time (RT) reaction cycles were run, following the manufacturer's instructions. The cDNA was then diluted, mixed with TaqMan Fast Advanced Master Mix (Thermo Fisher Scientific), and loaded onto the precoated Scorecard plates, which were then sealed and centrifuged at $600 \times g$ for 2 min. The RT-PCR cycles were run with the fast 96-well template on a QuantStudio 7 Flex RT-PCR System (Life Technologies Inc.). Quantitative RT-PCR array analysis was conducted on five batches of experimental samples from five different cell passages.

Cell Lineage Marker Protein Expression

To confirm whether the effects of MeHg on gene expression also occur at protein levels, we measured protein expression using western blots and enzyme-linked immunosorbent assays (ELISAs). hESCs were exposed to MeHg in six-well plates for 6 d, and protein extracts were obtained as described above. Immunoblotting of PVDF membranes was conducted using primary antibodies [1:1,000 in 3% BSA, except for natriuretic peptide B (NPPB), PR domain-containing protein 1 (PRDM1), paired box 3 (PAX3) and platelet-derived growth factor receptor-alpha (PDGFRA)] against human OCT4 (Catalog no. C30A3), SRY-box transcription factor 2 (SOX2; Catalog no. D6D9), Nanog homeobox (NANOG; Catalog no. D73G4; Cell Signaling Technology), NPPB (Catalog no. MBS9607555; MyBiosource) (1:500 in 5% NFDM), PAX3 (Catalog no. SAB2107888; Sigma-Aldrich) (1:1,000 in 5% NFDM), PDGFRA (Catalog no. PA5-16571) (1:500 in 5% NFDM), and PRDM1 (Catalog no. MA5-14879; Thermo Fisher Scientific) (1:500 in 5% NFDM), forkhead box A2 (FOXA2; Catalog no. ab108422), GATA binding protein 4 (GATA4; Catalog no. ab134057), Kruppel-like factor 5 (KLF5; Catalog no. ab137676), transient receptor potential cation channel subfamily M member 8 (TRPM8; Catalog no. ab3243; Abcam Inc.), SOX17 (Catalog no. AF1924), and cellular-MYC (Catalog no. MAB3696; R&D Systems) and HRP-linked goat antimouse (Catalog no. P0447; Dako), HRP-linked rabbit antigoat (P0160; Dako), or HRP-linked goat antirabbit (Catalog no. G-21234; Thermo Fisher Scientific) secondary antibody (1:5,000 in corresponding blocking buffer). The band intensities were quantified and normalized as described above. Because of logistics reasons, the protein expression of regulator of G protein signaling 4 (RGS4), dopamine receptor D4 (DRD4), and interleukin 6 cytokine family signal transducer (IL6ST) were measured using ELISAs with commercial kits from AVIVA Systems Biology (for RGS4, Catalog no. OKEI00172), and Life Span Biosciences (for DRD4, Catalog no. LS-F39474 and IL6ST, Catalog no. LS-F3388), according to manufacturer's instructions. Samples were diluted before analysis to ensure all sample absorbance values fell within the linear part of standard curves.

Statistical Analysis

All data were expressed as the means plus or minus the standard errors of the mean (means ± SEMs) and were tested for statistical significance with one-way ANOVA, followed by Dunnett's post hoc tests. The differences were considered significant if $p < 0.05$. Except for TaqMan Scorecard assay analysis, all statistical analyses were performed using GraphPad Prism (version 8; GraphPad).

For Scorecard analyses, CT values of target genes were subtracted by the CT values of the reference genes [Actin Beta (*ACTB*), CCCTC-binding factor (*CTCF*), E1A binding protein p300 (*EP300*), SMAD family member 1 (*SMAD1*)] to obtain ΔCT values. A cluster analysis was performed on the ΔCT values using the heatmap function in R version 3.6.1 (R Development Core Team). This cluster

analysis revealed that most samples within a batch were clustered together. Thus, a statistical model including the dose and batch factors on ΔCT (ΔCT = dose + batch) was applied using SAS Enterprise Guide 7.1 according to the method of Yuan et al. (2006). Using this model, each batch effect estimate was obtained. The ΔCT for each gene was subtracted by the batch effect estimate to give a derived ΔCT value for the gene. The same model (ΔCT = dose + batch) was used to estimate the gene expression difference between all MeHg dose groups and the control group based on ΔCT values. The level of probability of statistical significance was $p < 0.05$, where the p-value was adjusted by the Dunnett method for the multiple comparisons of 10 nM vs. 0 nM, 50 nM vs. 0 nM and 200 nM vs. 0 nM. Fold change was estimated using the function of $2^{(-\text{least square mean for MeHg dose group})}/2^{(-\text{least square mean for control})}$. Values for fold changes, probabilities of significance levels, and upper and lower 95% intervals of all genes are displayed in Excel Table S1.

Results

Cell Adhesion and Colony Formation in hESCs Exposed to MeHg for 6 d

Cell adhesion to the extracellular matrix is essential for hESCs to maintain intercellular communication, migration, viability, and proliferation. In the present study, we found that after 24 h of exposure to 200 nM MeHg, some hESCs lifted off the Matrigel, and those exposed to 500 nM MeHg were all floating (Figure 1A–H). After 3 d of exposure, the colony size and number in the 200 nM MeHg-treatment group were much smaller than those in the vehicle control group (Figure 1I–N). After 5 d of exposure, the same phenomenon was seen in all three of the 50, 100, and 200 nM MeHg dose groups (Figure 1O–T). After 6 d of exposure, colonies in the 200 nM MeHg-treatment group formed a multilayer structure with an evident peripheral membrane, a morphology markedly different from that of the vehicle control colonies (Figure 1U–W). The abnormal morphology was observed after 6 d of exposure at around 80% frequency, though the number of abnormal colonies in each batch was different. Another two batches of morphological images are provided in Figure S3.

Cell Viability and Proliferation in hESCs Exposed to MeHg for 6 d

After 24 h of exposure, cell viability in the hESCs treated with 200 nM MeHg was significantly lower than the vehicle control cells (Figure 2). This effect of 200 nM MeHg became more evident with the increasing duration of exposure from 24 h to 5 d (Figure 2). Significantly lower levels of cell viability were also detected in 10, 50, 100, and 200 nM MeHg-treated cells after 6 d of exposure compared with the control. The viability of the cells treated with 200 nM MeHg was the lowest at around 10% of control.

Intracellular Total Mercury Content in hESCs Exposed to MeHg for 24 h and 6 d

We observed higher levels of intracellular total mercury content in hESCs after 24 h and 6 d of MeHg exposure that appeared to be dose dependent in nature (Figure 3). However, the average amount of total mercury per cell was higher after 24 h than 6 d of exposure in the 50, 100, and 200 nM MeHg-dose groups.

Measurement of Apoptosis in hESCs Exposed to MeHg for 24 h and 6 d

After 24 h of exposure, the percentages of CC3-positive cells were significantly higher in 10, 50, and 200 nM MeHg-treated cells than vehicle control cells (Figure 4A), whereas no significant differences in the percentages of Annexin V-positive cells were observed between the MeHg-treatment group and the control group (Figure 4B). Some floating cells were observed in the culture media of all treatment groups, including the control group, every day before the medium change. The number of floating cells was significantly higher in the 200 nM MeHg-treated cells than the control groups after 24 h of exposure (Figure S4). There were no significant differences in the expression of CC3 among treatment groups (Figure 4C) after 6 d of exposure, whereas the percentages of Annexin V-positive cells in all MeHg-treatment groups were significantly higher than in the control group (Figure 4D).

Expression of Cytoskeletal Proteins in hESCs Exposed to MeHg for 6 d

We detected significantly higher protein expression of α-tubulin in hESCs exposed to 200 nM MeHg than the vehicle for 6 d (Figure 5A). For β-actin, there was no significant changes (Figure 5B).

ROS Presence and HO-1 Expression in hESCs Exposed to MeHg for 24 h or 6 d

We detected significantly higher levels of ROS in hESCs exposed to 200 nM MeHg vs. the vehicle for 24 h (Figure 6A). We observed higher HO-1 protein expression after 6 d of exposure in the same dose groups (Figure 6B). A trend of higher ROS levels and HO-1 expression was also observed in the lower MeHg-dose groups (Figure 6A,B). However, none reached a statistically significant level.

Measurement of Cell Cycle in hESCs Exposed to MeHg for 6 d

After 6 d of exposure, cells treated with 10, 50, and 200 nM MeHg showed significantly higher levels in the proportion of cells in the G1/S phase and lower levels in the proportion of cells in the G2 phase, compared with the cells treated with the vehicle (Figure 7A). These changes were associated with significantly higher protein levels of cyclin D1 (Figure 7B), but not cyclin A2 and E1 (Figures S5A and S5B), in the 200 nM MeHg-treated vs. the vehicle-treated cells.

Measurement of Autophagy Markers in hESCs Exposed to MeHg for 6 d

A lower LC3BII/LC3BI ratio (Figure 8A), accompanied by a higher expression of SQSTM1 (p62) (Figure 8B), was found in hESCs treated with 200 nM MeHg than those treated with the vehicle for 6 d. An image of the entire blot of LC3B with the ladder is provided in Figure S6.

Expression of Cell Lineage Markers in hESCs Exposed to MeHg for 6 d

We used Scorecard to examine the effects of MeHg on the expression of 82 cell lineage marker genes after 6 d of exposure (Excel Table S1 and S2). Our data revealed that the gene expression profile in the 200 nM MeHg-treated hESCs clustered away from the profile of all other dose groups (Figure 9A). In addition, the self-renewal genes clustered together, whereas other cell lineage marker genes were distributed in other clusters with no obvious cell lineage separation (Excel Table S2). Cells treated with each of the three doses (10, 50, and 200 nM) of MeHg exhibited significant differences in the expression of one or more cell lineage marker genes; cells treated with 10 nM exhibited one differentially expressed gene, cells treated with 50 nM exhibited

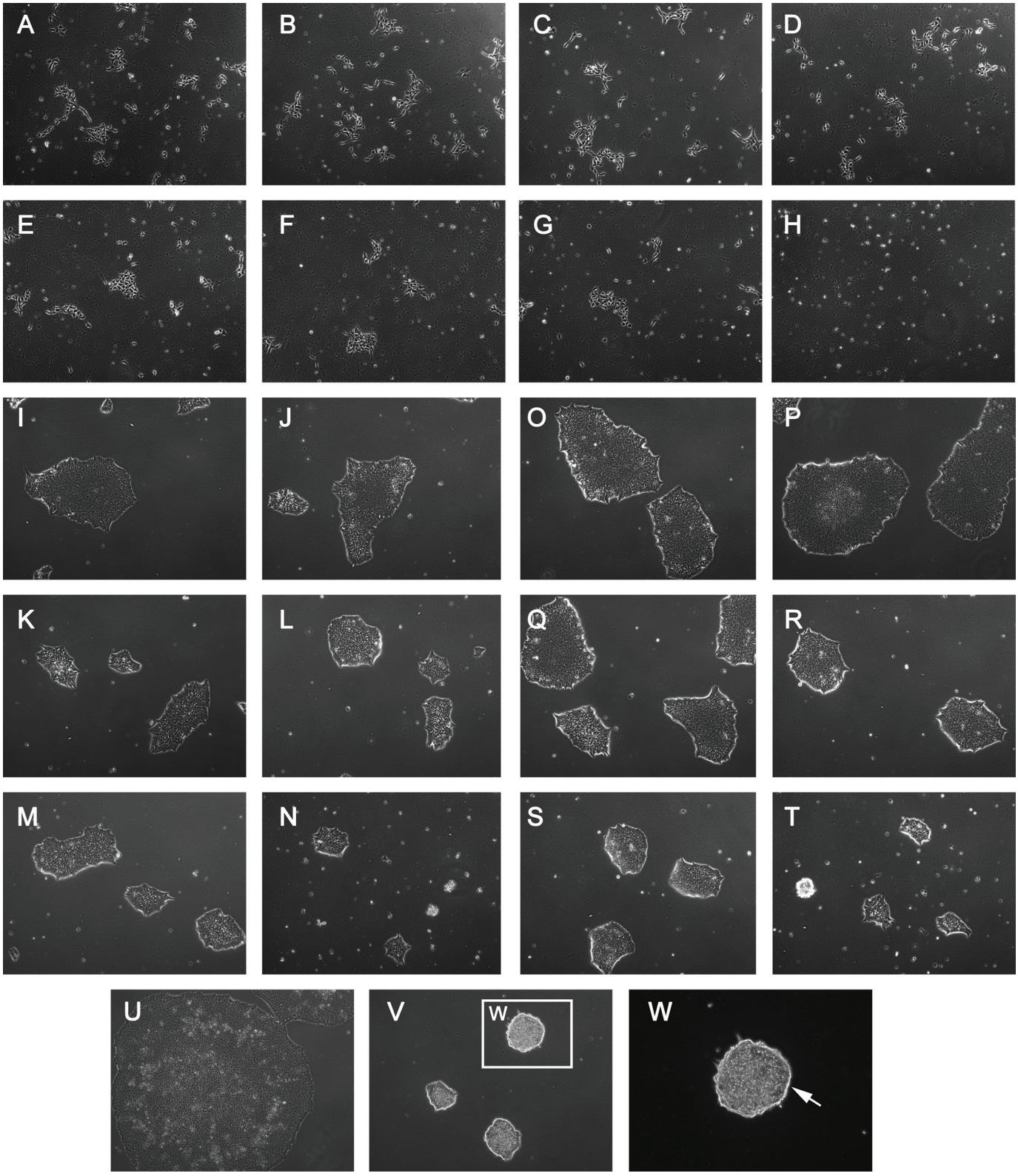

Figure 1. The effect of MeHg exposure on the cell attachment, colony formation, and morphology of hESCs. Representative images showing cellular attachment and colony formation of hESCs after 24 h of exposure to (A) 0, (B) 1, (C) 5, (D) 10, (E) 50, (F) 100, (G) 200, and (H) 500 nM MeHg, and colony size or morphology of hESCs after 3 d of exposure to (I) 0, (J) 5, (K) 10, (L) 50, (M) 100, and (N) 200 nM MeHg, after 5 d of exposure to (O) 0, (P) 5, (Q) 10, (R) 50, (S) 100, and (T) 200 nM MeHg, or after 6 d of exposure to (U) 0 and (V and W) 200 nM MeHg. (A–V) were taken under a 10× objective. (W) is the Zoom-in of (V) and which was taken under a 20× objective. At least five wells with at least five fields were observed, and at least three images were taken for each treatment group. The arrow indicates the peripheral membrane of the multilayer structure. Note: hESC, human embryonic stem cell; MeHg, methylmercury.

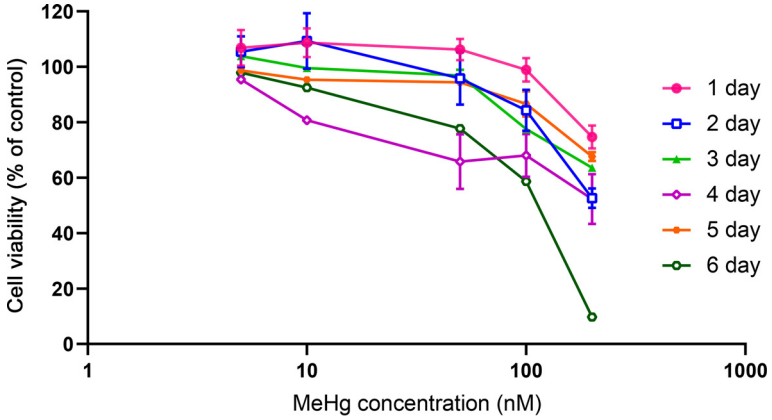

Figure 2. Effects on cell viability of hESCs exposed to MeHg for 24 h to 6 d. Cell viability of each dose at each time point was adjusted to the respective sodium carbonate vehicle control. One-way ANOVA was used at each time point to compare between the different doses and the dose response of the treatment effects was significant. Dunnett's post hoc test was then used to compare the treatments to the vehicle control. Significance was set at $p < 0.05$. Data are presented as means ± SEMs with $n = 4$ for each group. Five-nanomolar MeHg showed significantly higher cell viability on Day 3; 10 nM MeHg showed significantly lower cell viability on Day 6; 50 nM MeHg showed significantly lower cell viability on Days 4 and 6; 100 nM MeHg showed significantly lower cell viability on Days 3–6; and 200 nM MeHg showed significantly lower cell viability at all time points. The corresponding numeric data are provided in Table S1. Note: ANOVA, analysis of variance; hESC, human embryonic stem cell; MeHg, methylmercury; SEM, standard error of the mean.

three differentially expressed genes, and cells treated with 200 nM exhibited nine differentially expressed genes (Figure 9B–G). Expression of *IL6ST* (a mesoderm gene) was significantly higher in all three MeHg-dose groups compared with the control. Expressions of *PAX3* (an ectoderm gene) and *KLF5* (an endoderm gene) was significantly lower in the 50 nM MeHg-treatment group than in the control group. Expressions of myosin IIIB [*MYO3B* (an ectoderm gene)], *FOXA2* (an endoderm gene), *PDGFRA* (a mesoderm gene), and *OCT4* [*POU5F1* (a self-renewal gene)] were significantly higher in the 200 nM MeHg-treatment group than in the control group. In contrast, the expressions of *KLF5*, *PRDM1* (an endoderm gene), *NPPB* (a mesendoderm gene), and *MYC* (a noncell lineage-related gene) were significantly lower in the 200 nM MeHg-treatment group than in the control group. Expressions of *SOX2*, *CXCL5*, and *DNMT3B* (all self-renewal genes) were also higher in the 200 nM MeHg-treatment group than the in control group but did not reach statistically significant levels.

At the protein level, we found higher levels of OCT4 (Figure 10A) in the 50 nM and 200 nM MeHg-treatment groups after 6 d of exposure. Five other proteins, including two self-renewal proteins [NANOG (Figure 10B) and SOX2 (Figure 10C)], two endoderm proteins [GATA4 (Figure 10D) and PRDM1 (Figure 10E)], and a mesoderm protein [IL6ST (Figure 10F)] were all higher in the 200 nM MeHg-treated cells only. We found no significant difference in the protein expression of FOXA2, KLF5, PAX3, TRPM8, c-MYC, SOX17, PDGFRA, NPPB, RGS4, and DRD4 in the hESCs treated with MeHg compared with the control group (Figure S7). Therefore, only OCT4, PRDM1, and IL6ST showed significant differences at both gene and protein levels in the

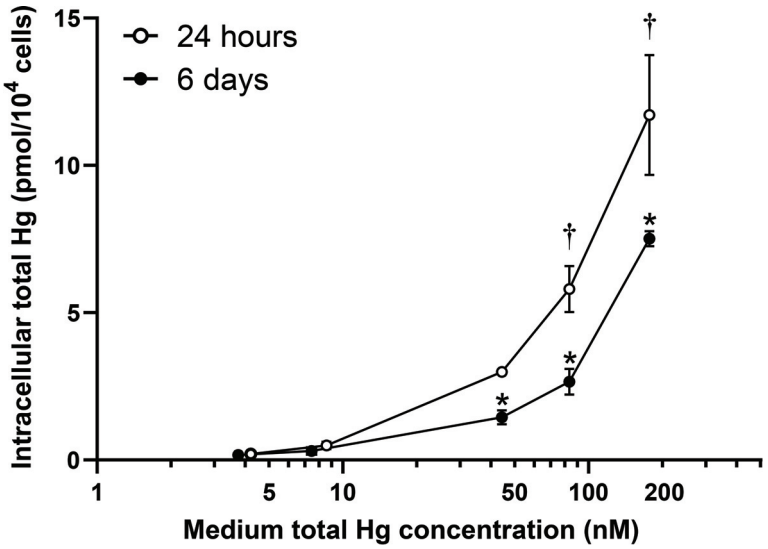

Figure 3. Intracellular total mercury content in hESCs exposed to MeHg for 24 h and 6 d. One-way ANOVA was used at each time point to compare between the different doses, and the dose response of the treatment effects was significant. Dunnett's post hoc test was then used to compare the treatments to the sodium carbonate vehicle control. Significance was set at $p < 0.05$. Data are presented as means ± SEMs with $N = 3$ for each group. The values <0 were regarded as 0. †, $p < 0.05$ within 24 h. *, $p < 0.05$ within 6 d. Values on the *x*-axis represent actual total mercury concentrations measured in culture medium dosed with 5, 10, 50, 100, and 200 nM MeHg for 24 h or 6 d, respectively. The doses shown in the figure were the measured concentrations in the media. The corresponding numeric data are provided in Table S2. Note: ANOVA, analysis of variance; hESC, human embryonic stem cell; Hg, mercury; MeHg, methylmercury; SEM, standard error of the mean.

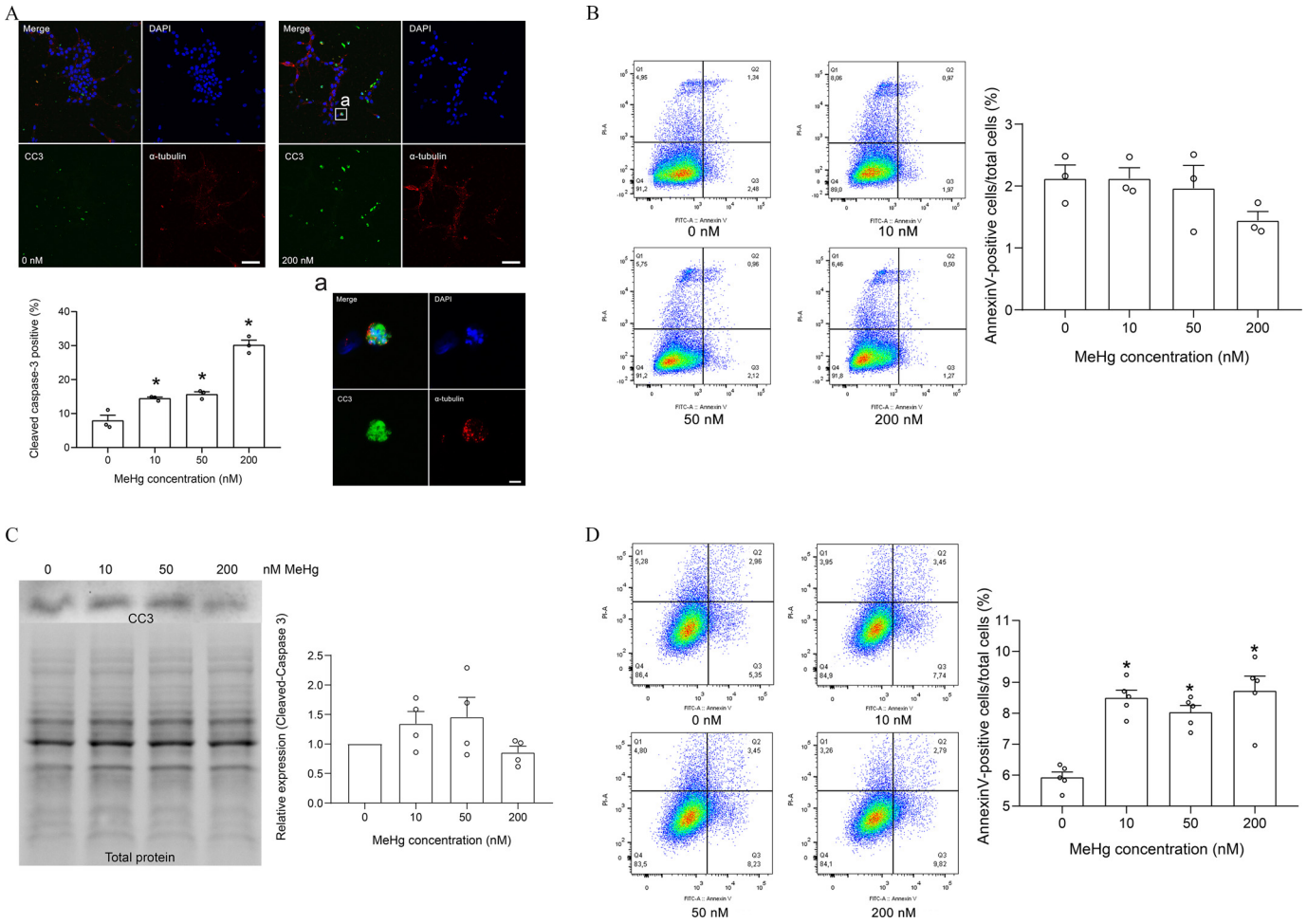

Figure 4. Measures of apoptosis in hESCs exposed to MeHg for 24 h and 6 d. (A) Representative image of positive staining of cleaved caspase-3 (CC3) (green), nuclei (DAPI, blue) and α-tubulin (red) and quantification of CC3-positive cells (as a percentage of nuclei) in hESCs exposed to 0 and 200 nM MeHg for 24 h. Scale bar: 100 µm; scale bar in the Zoom-in of (A): 10 µm. (B) Flow cytometry analysis of cell population (percentage) positively stained for Annexin V-FITC and propidium iodide (PI) as measures of early apoptosis and necrosis after 24 h of MeHg treatment, respectively. (C) Expression of CC3 protein after 6 d of MeHg exposure. Each batch was first normalized to its sodium carbonate vehicle control (0 nM) before comparison. Thus, there is no error bar in the 0 nM MeHg group. (D) Flow cytometry analysis of cell population (percentage) positively stained for Annexin V-FITC and PI as measures of early apoptosis and necrosis after 6 d of MeHg treatment, respectively. Data are presented as means ± SEMs with $N = 3$ for immunostaining and flow cytometry (24 h), $N = 4$ for western blot, and $N = 5$ for flow cytometry (6 d). The small circle symbols represent individual values of each experiment. One-way ANOVA was used at each time point to compare between the different doses, and the dose response of the treatment effects was significant for (A) CC3 expression at 24 h and (D) Annexin V-positive cells at 6 d. Dunnett's post hoc test was then used to compare the treatments to the vehicle control. Significance (*) was set at $p < 0.05$. The corresponding numeric data are provided in Table S3. Note: ANOVA, analysis of variance; DAPI, 4′,6-diamidino-2-phenylindole; FITC, fluorescein-5-isothiocyanate; hESC, human embryonic stem cell; MeHg, methylmercury; SEM, standard error of the mean.

200 nM MeHg-treated cells compared with control cells. In addition, the protein expressions of another two self-renewal makers [SOX2 (Figure 10C) and NANOG (Figure 10B)] were also significantly higher in 200 nM MeHg-treated cells even though no significant difference was detected in the gene expression levels of these two markers (Figure 9B; Excel Table S1).

Discussion

Previous studies looking at the effects of MeHg on embryo development focused mostly on the neural system. Little is known about the effects of MeHg on the physiology of undifferentiated hESCs. In humans, implantation starts from about Day 7–8 and basically completes at around Day 12 after fertilization (Lenton et al. 1982; Lopata 1996). Because many pregnancies are unplanned, it is important to understand the effects of MeHg at this early stage of embryo development, particularly for risk assessment for fish-consuming populations. Our observed low-dose effects of MeHg in undifferentiated hESCs cultured under the physiologically relevant O_2 conditions after 24 h or 6 d of exposure were planned to mimic the acute (24 h exposure) and continuous *in vivo* MeHg exposure throughout the pre-, during, and early postimplantation stages of embryo development (6-d exposure) (Figure 11). Our results showed dose–response effects of nanomolar concentrations of MeHg on hESC colony morphology, cell viability, proliferation, apoptosis, stress response, cytoskeleton protein expression, autophagy, cell cycle, and expression of various cell lineage marker genes/proteins. The significance of this observation in the physiopathology of spontaneous abortions warrants further study.

Conducting toxicology experiments using undifferentiated hESCs presents many challenges in both the methodology and the interpretations of results. hESCs were isolated from the ICM of human blastocysts. ICM cells have relatively high natural apoptotic rates as the result of an eliminative process that helps trim the embryonic cell lineages of surplus or dysfunctional stem cells (Huppertz and Herrler 2005; Pampfer and Donnay 1999). Undifferentiated hESCs have a primed death machinery with Bax

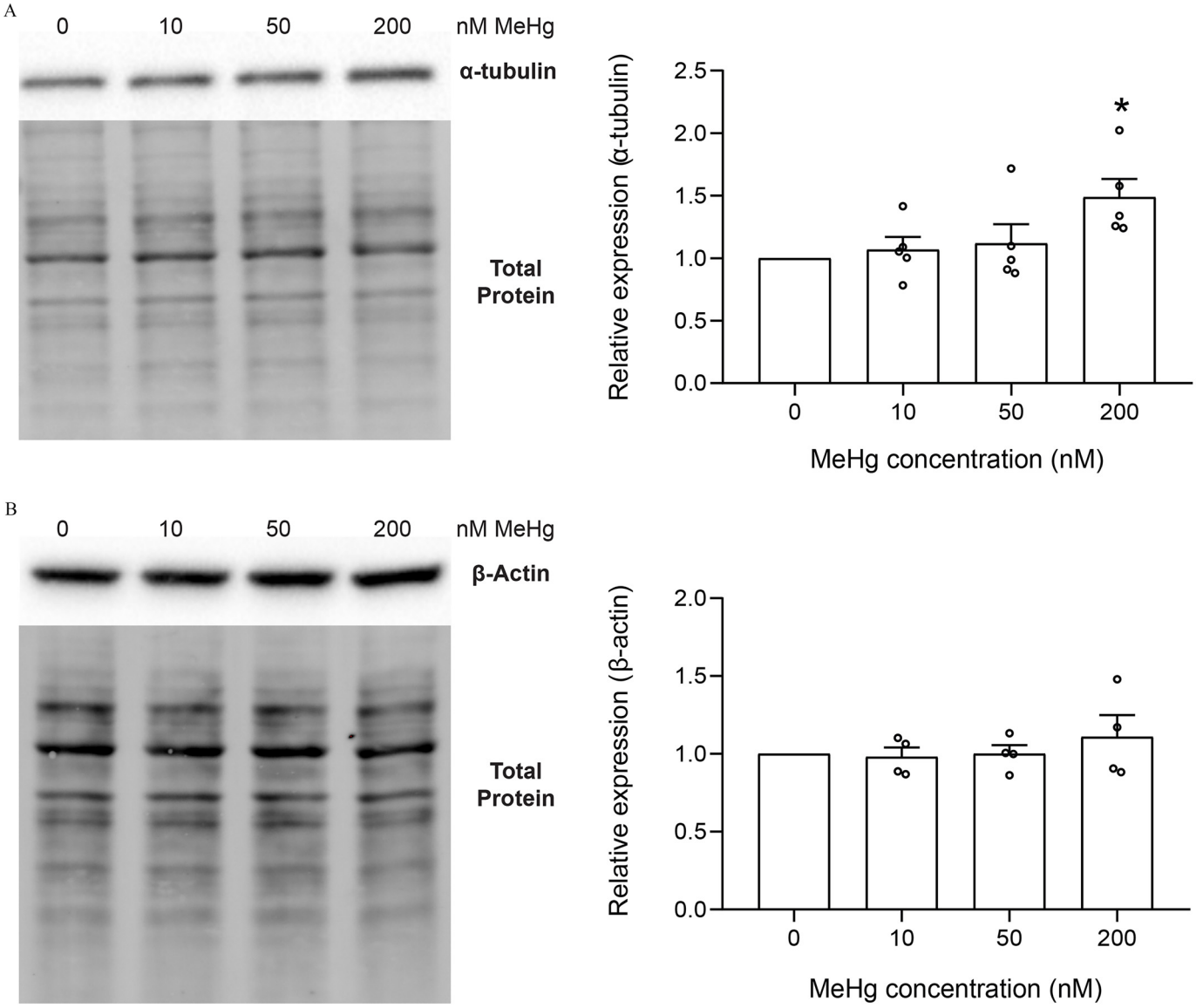

Figure 5. Expressions of (A) α-tubulin and (B) β-actin proteins in hESCs exposed to 0, 10, 50, and 200 nM MeHg for 6 d. Data are presented as means ± SEMs with $N = 5$ for α-tubulin and $N = 4$ for β-actin. Each batch was first normalized to its sodium carbonate control (0 nM) before comparison. Thus, there are no error bars in the 0 nM MeHg groups. The small circle symbols represent individual values of each experiment. One-way ANOVA was used at each time point to compare between the different doses, and the dose response of the treatment effects was significant for (A) expression of α-tubulin. Dunnett's post hoc test was then used to compare the treatments to the vehicle control. Significance (*) was set at $p < 0.05$. The corresponding numeric data are provided in Table S4. Note: ANOVA, analysis of variance; hESC, human embryonic stem cell; MeHg, methylmercury; SEM, standard error of the mean.

already active, which rapidly translocate from the Golgi to the mitochondria upon DNA damage, where they exert apoptosis within hours (Dumitru et al. 2012). In the present study, we observed floating cells every day, even in the control group before the daily medium change, and the number of floating cells was higher in wells with cells that had been treated with MeHg. This effect of MeHg treatment on cell adhesion has also been reported previously (Jayashankar et al. 2011). The reduced cell adhesion may be caused by lower cell viability or by a change in cellular adherent molecules—such as integrins, cadherins, and selectins—leading to a rearrangement of cell skeleton structures (Coleman and Olson 2002) and disruption of cell junctions. Therefore, all the results reported are on the cells that survived might have developed selective resistance mechanisms.

The viability of cultured hESCs decreased with time and MeHg concentrations (Figure 2). On Day 6, the cell viability was ~90% at 10 nM, 80% at 50 nM, and 10% at 200 nM relative to the control. These results suggest that undifferentiated hESCs are as vulnerable to MeHg toxicity as the neural stem cells. For example, exposure to MeHg at 50 nM caused a 50% reduction in cell viability and proliferation in human embryonic neural progenitor cells after 20 h of exposure accompanied by an increase in ROS production and apoptosis (Wang et al. 2016) and MeHg at ≥50 nM significantly decreased cell viability in hESCs after 12 d of exposure (Stummann et al. 2009). We measured cell viability and proliferation using the WST assay. This assay measures the formation of formazan from WST-1 and requires the action of mitochondrial dehydrogenase present in the metabolically active cells, thus reflecting cell viability and proliferation. Because MeHg acts on sulfhydryl (SH–) groups and may decrease the mitochondrial dehydrogenase activity by directly binding to SH– groups in proteins or indirectly by ROS-induced oxidation of SH– groups, the WST assay values may reflect the combined effects of MeHg on cell viability, cell proliferation, and mitochondrial dehydrogenase.

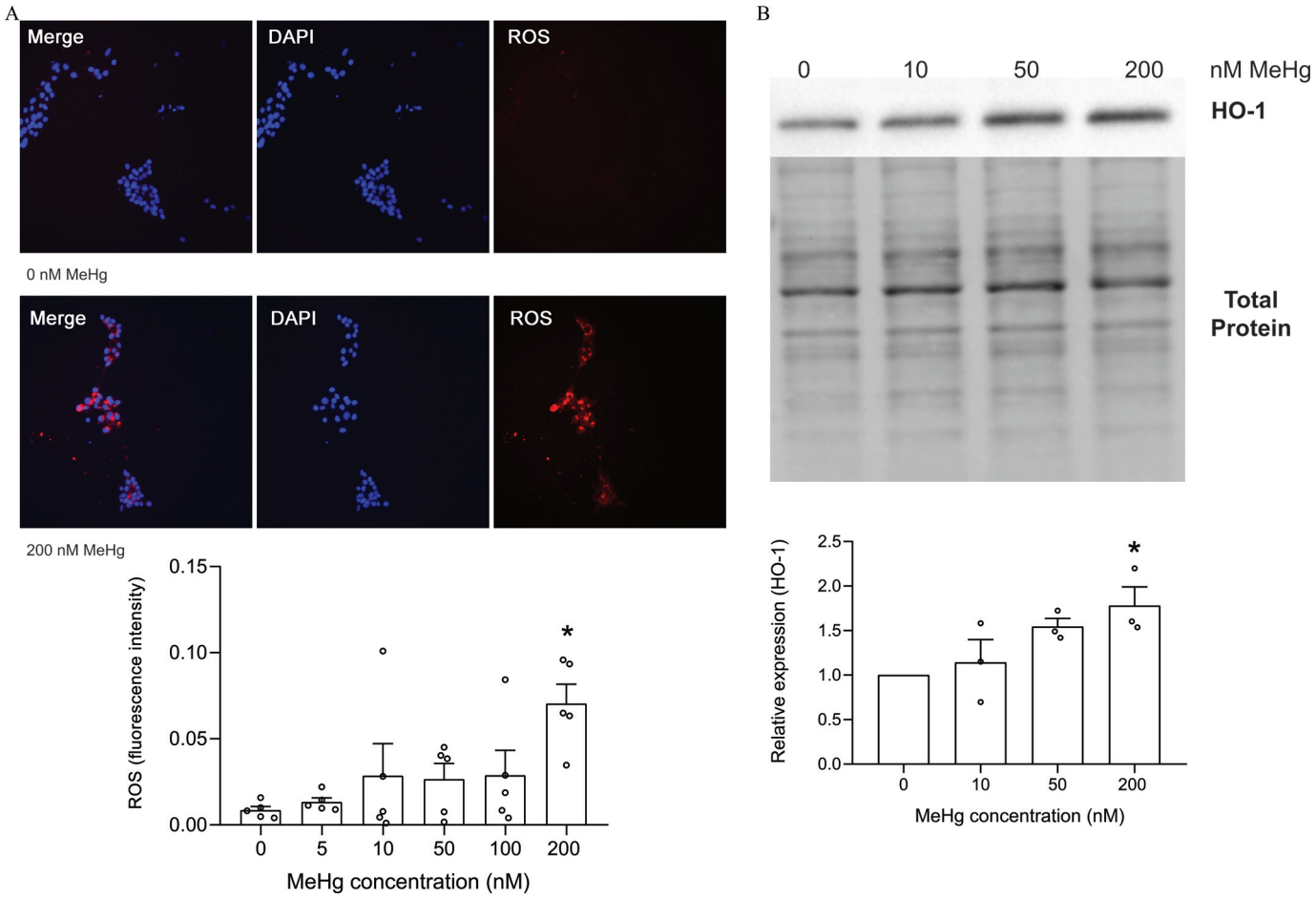

Figure 6. Presence of (A) reactive oxygen species (ROS) and (B) protein expression of HO-1 in hESCs exposed to MeHg for 24 h and 6 d, respectively. Microscopic images are DAPI staining of nuclei (blue) and CellRox staining of ROS (red). Data are presented as means ± SEMs with $N = 5$ for ROS fluorescence intensity and $N = 3$ for HO-1 western blots. For western blots, each batch was first normalized to its sodium carbonate vehicle control (0 nM) before comparison. Thus, there are no error bars in the 0 nM MeHg groups. The small circle symbols represent individual values of each experiment. One-way ANOVA was used at each time point to compare between the different doses, and the dose response of the treatment effects was significant. Dunnett's post hoc test was then used to compare the treatments to the vehicle control. Significance (*) was set at $p < 0.05$. The corresponding numeric data are provided in Table S5. Note: ANOVA, analysis of variance; DAPI, 4′,6-diamidino-2-phenylindole; hESC, human embryonic stem cell; HO-1, hemeoxygenase-1; MeHg, methylmercury; SEM, standard error of the mean.

Therefore, the estimate of cell death, particularly at 200 nM MeHg, may be overestimated. Nevertheless, the increase of ROS and HO-1 levels showed that those cells were under stress and that the MeHg treatment clearly decreased proliferation. After 6 d of exposure, cells treated with 10, 50, and 200 nM MeHg all showed a higher proportion of cells in G1/S phase and less in G2 phase and showed higher levels of cyclin D1 (Figure 7). Similar observations were reported by Burke et al. (2006) and Xu et al. (2010) in cortical progenitor cells. This could be a result of an increase in ROS-induced DNA damage, leading to activation of checkpoint and DNA repair processes in the G1/S phase, preventing the transition of cells from the G1/S to the G2 phase. The higher level of α-tubulin expression in 200 nM MeHg-treated cells is also consistent with the changes in cell cycle dynamics observed in these cells. It has been demonstrated that the cell cycle machinery is directly involved in the transcriptional initiation of developmental genes controlling primary germ layer specification (Pauklin and Vallier 2015). hESCs in the early G1 phase can only initiate differentiation into endoderm, whereas hESCs in the late G1 phase are limited to neuroectoderm differentiation (Pauklin and Vallier 2013).

MeHg has been reported to increase apoptosis in mouse neural progenitor cells after 3 h of exposure at 100 nM (Watanabe et al. 2013). Our results also showed that apoptosis was important in MeHg-mediated cell death in hESCs and that it also played a significant role in the selection of resistant hESCs. There appear to be inconsistencies in our results for apoptosis measured by two different markers—CC3 and Annexin V—in the hESCS at 24 h and Day 6. CC3 showed MeHg treatment effects at 24 h but not at Day 6, whereas Annexin V showed MeHg treatment effects at Day 6 but not at 24 h (Figure 4). This could be due to a number of factors. First, the percentage of CC3-positive cells for 24 h exposure was measured by immunocytochemical staining and by western blot at Day 6 because the cells grew into multiple layers after 6 d of exposure. Second, the higher rate of apoptosis (indicated by CC3) in the 200 nM MeHg-treated group after 24 h compared with 6 d of exposure could be explained as *a*) the cells that survived at Day 6 were more resistant to MeHg; *b*) given that the cell density increased from 1×10^4cells/mL at 24 h to $5–20 \times 10^4$cells/mL at Day 6, the effective dose of MeHg that each cell was exposed to was lower at 24 h than Day 6 (the measured total mercury per cell was higher at 24 h than at Day 6); and *c*) the cells that could show high expression of CC3 had been removed with the medium change (Figure S4), and the cells that survived at 6 d were protected from MeHg exposure by forming more compact, multilayered, smaller colonies. Third, at 24 h, the cells could be at the middle/late stage of apoptosis and that could

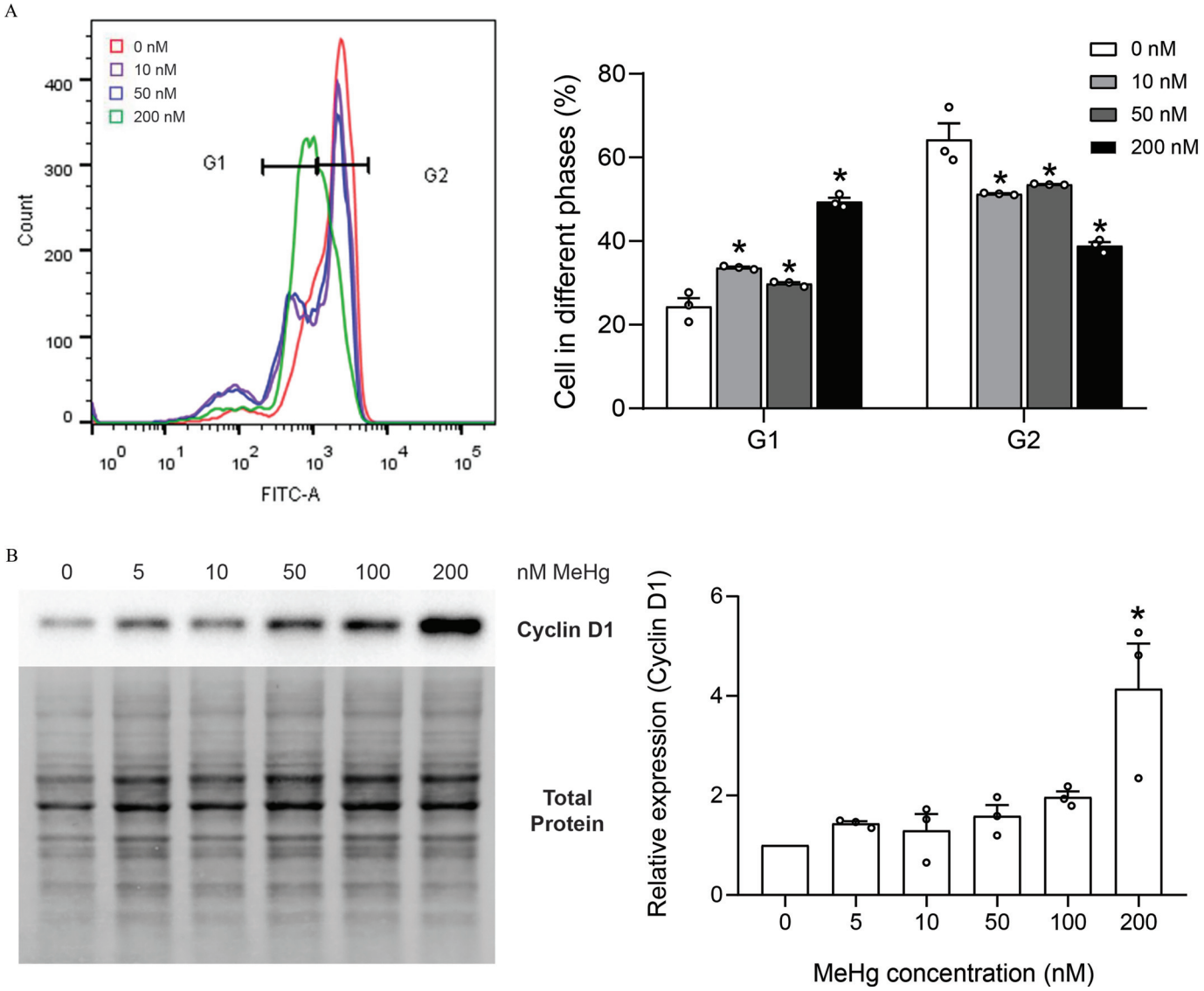

Figure 7. Analysis of the cell cycle of hESCs after 6 d of exposure to MeHg. (A) Flow cytometry analysis of cell cycle phases, with a histogram showing the peak for FITC-staining of DNA content as identifications of cell phases and bar graph showing the percentage of cells in different cell cycle phases of hESCs after 6 d of exposure to 0, 10, 50, and 200 nM MeHg. (B) Protein expression of cyclin D1 was measured in hESCs after 6 d of exposure to 0, 5, 10, 50, 100, and 200 nM MeHg. Data are presented as means ± SEMs with $N = 3$ for each group. For western blots, each batch was first normalized to its sodium carbonate vehicle control (0 nM) before comparison. Thus, there is no error bar in the 0 nM MeHg group. The small circle symbols represent individual values of each experiment. One-way ANOVA was used at each time point to compare between the different doses, and the dose response of the treatment effects was significant. Dunnett's post hoc test was then used to compare the treatments to the vehicle control. Significance (*) was set at $p < 0.05$. The corresponding numeric data are provided in Table S6. Note: ANOVA, analysis of variance; FITC, fluorescein-5-isothiocyanate; hESC, human embryonic stem cell; MeHg, methylmercury; SEM, standard error of the mean.

be shown by the CC3 but not the Annexin V, which stained for an earlier stage of apoptosis. At Day 6, the surviving cells were more resistant and did not undergo further middle/late apoptosis and hence showed more positive staining for Annexin V. The cells that survived at 6 d of MeHg treatment also had higher expression of self-renewal gene *OCT4*, and proteins OCT4, SOX2 and NANOG. It remains to be determined if these cells would be able to implant and develop further *in vivo*.

Even though the underlying molecular mechanisms for MeHg toxicity are not completely understood, much evidence indicates MeHg toxicity is mediated by its pro-oxidative properties (Farina and Aschner 2017). We observed a higher level of ROS after 24 h of 200 nM MeHg exposure, similar to that reported in human embryonic neural progenitor cells (Wang et al. 2016), which could be attributed to the induction of the uncoupling of the mitochondrial electron transport chain or depletion of reduced glutathione (Gatti et al. 2004; Mori et al. 2011). Given that the hESCs were maintained at a physiologically relevant O_2 level (4%) in the present study, they had not adapted to the atmospheric O_2 environment ($\sim$20%) and thus were prone to ROS damage induced by MeHg, resulting in increased apoptosis. The conjugation of SH– groups with MeHg could also contribute to cell death by inhibiting enzymatic activity related to DNA replication, carbohydrate and lipid metabolism, and heme synthesis (Ajsuvakova et al. 2020). Another possible mechanism is the modulation of autophagy and apoptosis. We observed that MeHg treatment caused a decrease in autophagy, indicated by a lower LC3BII/LC3BI ratio and higher protein expression of p62 with the increase in apoptosis, as reported in the anterior pituitary of rats (El Asar et al. 2019). Therefore, the MeHg treatment effect may be mediated through a similar mechanism of

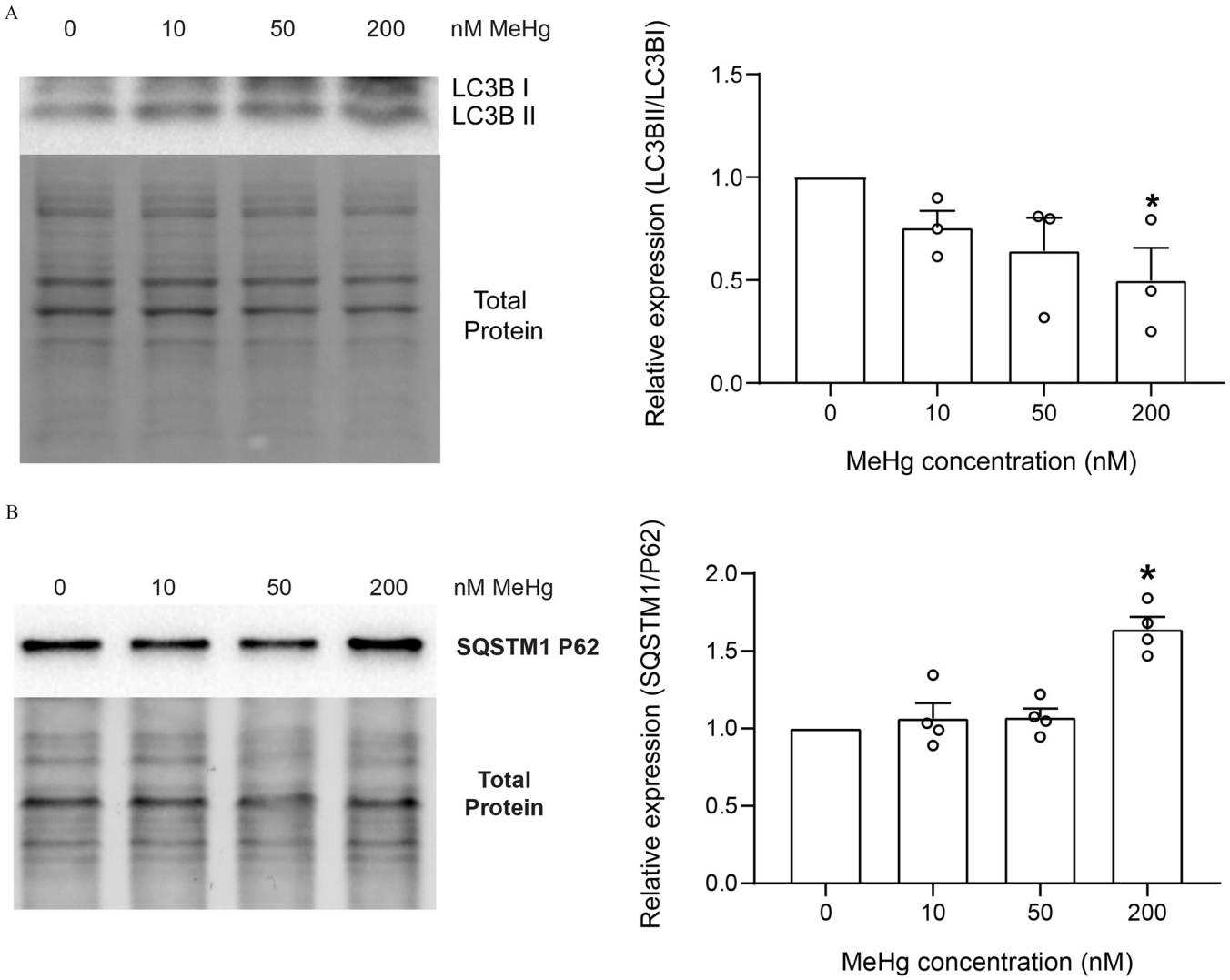

Figure 8. Protein expressions of LC3B (LC3BI and LC3BII) and SQSTM1 (p62) were measured in hESCs after 6 d of exposure to 0, 10, 50, and 200 nM MeHg. Data are presented as means ± SEMs with $N = 3$ for LC3B and $N = 4$ for SQSTM1 (p62). For LC3B, the ratio of LC3BII/LC3BI was calculated first before comparison. Each batch was first normalized to its sodium carbonate vehicle control (0 nM) before comparison. Thus, there are no error bars in the 0 nM MeHg groups. The small circle symbols represent individual values of each experiment. One-way ANOVA was used at each time point to compare between the different doses, and the dose response of the treatment effects was significant. Dunnett's post hoc test was then used to compare the treatments to the vehicle control. Significance (*) was set at $p < 0.05$. The corresponding numeric data are provided in Table S7. Note: ANOVA, analysis of variance; hESC, human embryonic stem cell; LC3B, microtubule-associated proteins 1A/1B light chain 3B; MeHg, methylmercury; SEM, standard error of the mean; SQSTM1 (p62), sequestosome 1.

causing a blockage of autophagy, augmenting the apoptotic profile and leading to the release of pro-apoptotic cell mediators, thereby increasing mitochondrial membrane permeability and promoting cell death. The most recent advances in the comprehension of the functions of autophagy pathways suggest that autophagy is a decision maker between quiescence, self-renewal, and differentiation in physiological vs. pathological conditions (Rodolfo et al. 2016). mTOR, a negative regulator of autophagy (Wang and Zhang 2019), supports long-term self-renewal and suppresses mesoderm and endoderm differentiation in hESCs (Zhou et al. 2009). Spontaneous and induced differentiation promote autophagy in the hESC cell line HES3 LC3-GFP (Tra et al. 2011). Chaperone-mediated autophagy (CMA) is up-regulated during differentiation of mouse ESCs (Xu et al. 2020), whereas pluripotency factors OCT4 and SOX2 suppresses CMA (Xu et al. 2020). These observations also support our findings that the cells that survived 6 d of MeHg treatment had decreased autophagy, measured as the decreased ratio of LC3BII/LC3BI (Yuntao et al. 2016) and the increased protein expression of SQSTM1 (p62) (Rusten and Stenmark 2010), which paralleled with increased expression of self-renewal genes and proteins. Normally, GATA4 is degraded by autophagy, so the observed increase in GATA4 in the 200 nM MeHg-treated hESCs may be caused by the observed autophagy inhibition and may lead to a possible initiation of the senescence-associated secretory phenotype (Kang et al. 2015).

It is important to note that the uniqueness of the present study is in investigating the properties of the undifferentiated cell population in the cell culture system. The hESCs were grown in Essential 8 Flex Medium that was formulated to support and maintain pluripotency and was lacking factors required for germ layer differentiation. Therefore, the levels of lineage gene expression are expected to be small, and very minor shifts in the cell population can result in very large changes in marker gene expression. Nevertheless, our results in cell lineage markers at both gene and protein expression levels provide preliminary evidence on the mechanisms of MeHg toxicity. For example, we found that hESCs exposed to 200 nM MeHg had markedly higher cyclin D1 expression, which is consistent with the higher

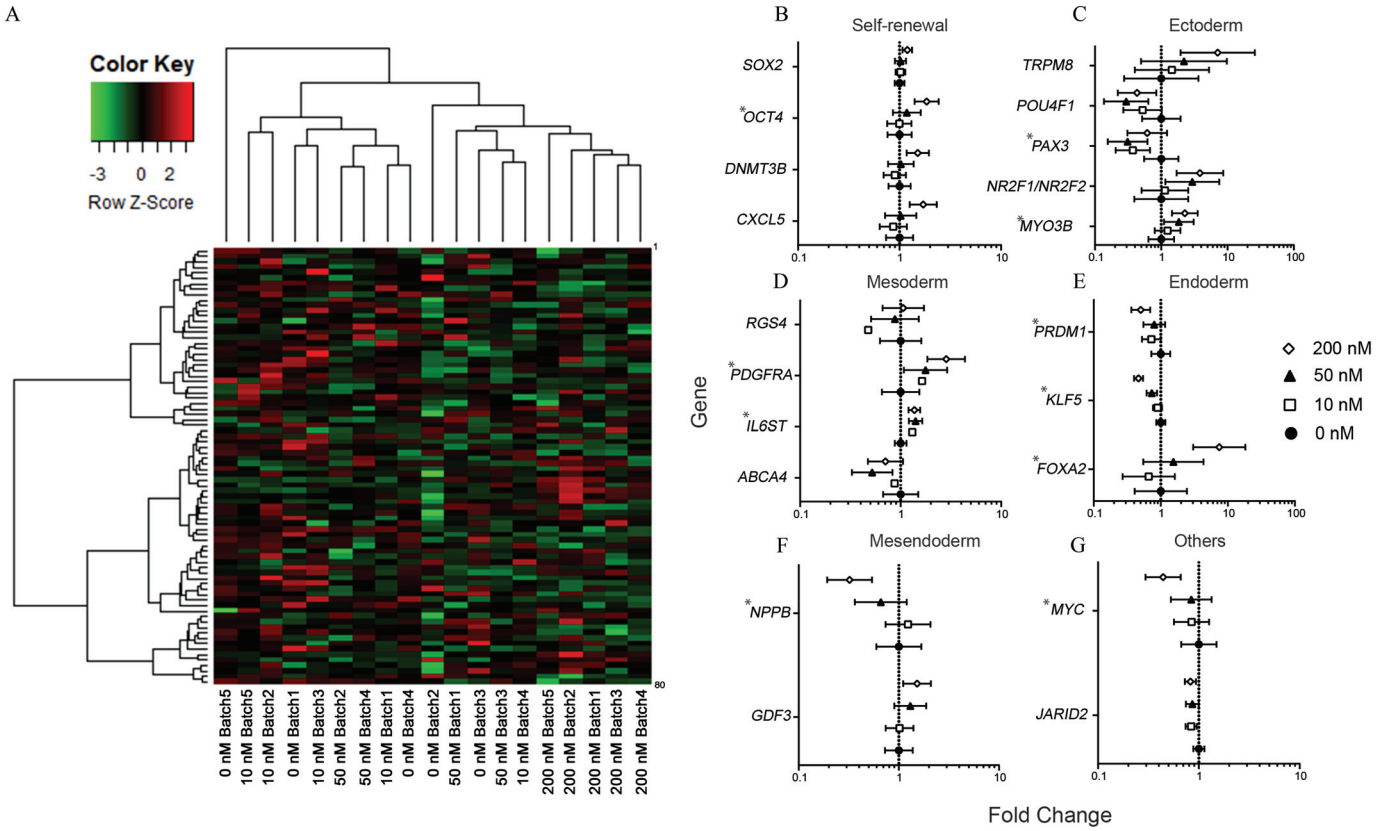

Figure 9. Hierarchical cluster analysis and fold change estimates of cell lineage marker gene expression data. (A) A cluster analysis was carried out using the heatmap function in R for the derived ΔCT values, as described in the "Materials and Methods" section. Rows represent genes, and columns represent samples. Red and green blocks respectively represent high and low expression relative to the reference gene, whereas black blocks indicate equal expression. (B–G) The expression of genes with significant difference between the MeHg-treatment groups and the control group. Fold change was estimated using the function of $2^{(-\text{least square mean for MeHg dose group})}/2^{(-\text{least square mean for control})}$. Data are presented as mean fold change $\pm 95\%$ CI with $N = 5$ for each group. The dashed line in each panel represents the line of no fold change. An asterisk indicates genes that remain significant (adjusted $p < 0.05$) after controlling for batch effect using a statistical model (ΔCT = dose + batch), as described in the "Materials and Methods" section. The corresponding numeric data are provided in Excel Table S1. Note: *ABAC4*, ATP Binding Cassette, Subfamily A, Member 4; CI, confidence interval; *CXCL5*, C-X-C Motif Chemokine Ligand 5; *DNMT3B*, DNA Methyltransferase 3 Beta; *FOXA2*, forkhead box A2; *GDF3*, Growth Differentiation Factor 3; *IL6ST*, interleukin 6 cytokine family signal transducer; *JARID*, Jumonji/ARID domain-containing protein 2; *KLF5*, Kruppel-like factor 5; MeHg, methylmercury; *MYC*, Myc proto-oncogene protein; *MYO3B*, myosin IIIB; *NPPB*, natriuretic peptide B; *NR2F1/NR2F2*, Nuclear receptor subfamily 2, group F, member 2/member 1; *OCT4*, octamer-binding transcription factor 4; *PAX3*, paired box 3; *PRDM1*, PR domain-containing protein 1; *PDGFRA*, platelet-derived growth factor receptor-alpha; *POU4F1*, POU domain, class 4, transcription factor 1; *RGS4*, protein expression of regulator of G protein signaling 4; *SOX2*, SRY-box transcription factor 2; *TRPM8*, transient receptor potential cation channel subfamily M member 8.

expression of self-renewal genes and proteins observed under the same condition. Cyclin D1, which is highly expressed in the late G1 phase, recruits transcriptional corepressors to endoderm genes, thereby blocking the induction of the corresponding germ layers (Pauklin et al. 2016). There is evidence demonstrating that a proper level of Cyclin D is necessary for maintaining the pluripotent state of ESCs, whereas its overexpression may induce reprogramming of epidermal cells into stem-like cells with higher expression of OCT4 (She et al. 2017; Zhao et al. 2016). These changes may prevent the hESCs from germ layer lineage commitment, which, if it occurs *in vivo*, would result in miscarriage. Varum et al. (2009) found inhibition of mitochondrial respiratory chain enhanced pluripotency measured by OCT4 expression in hESCs. Therefore, our observed higher expression of OCT4 at both the gene and protein level in the 200 nM MeHg-treated cells could also be caused by a similar disruption of the mitochondria respiratory chain by MeHg. OCT4 is a transcription factor vital for maintaining ESC pluripotency and plays a coordinating role in the G1/S phase transition by regulating the expression of cyclin D and cyclin E (She et al. 2017). Therefore, OCT4 may also play a key role in the observed increased expression of cyclin D and cell cycle arrest at the G1/S phase in the hESCs. The SOX2 expression may also relate to the higher expression of cyclin D1 and cell cycle arrest, as suggested by others (Card et al. 2008; Li et al. 2017). Our finding of the higher expression of OCT4, SOX2, and PRDM1 in the 200 nM HgMg-treated hESCs is interesting because the development from pluripotent stem cells to primordial germ cells is driven by switching partners with OCT4 from SOX2 to PAX5, resulting in the up-regulation of PRDM1 (Fang et al. 2018). Given that the dysregulation of genetic pathways during human germ cell development can lead to infertility, the effects of MeHg on the core transcriptional network of PAX5–OCT4–PRDM1 proteins that activates germline and represses somatic programs during human germ cell differentiation should be further investigated. Both IL6ST and NANOG are known to play important roles in the maintenance of self renewal of ESCs *in vitro* (Hu et al. 2009; Saunders et al. 2013). The fact that cells exposed to MeHg had a simultaneously higher expression of IL6ST and three self-renewal markers OCT4, SOX2, and NANOG shows that exposure of hESCs to MeHg at the blastocyst stages could inhibit or delay the differentiation of the three germ layers and increase the risk

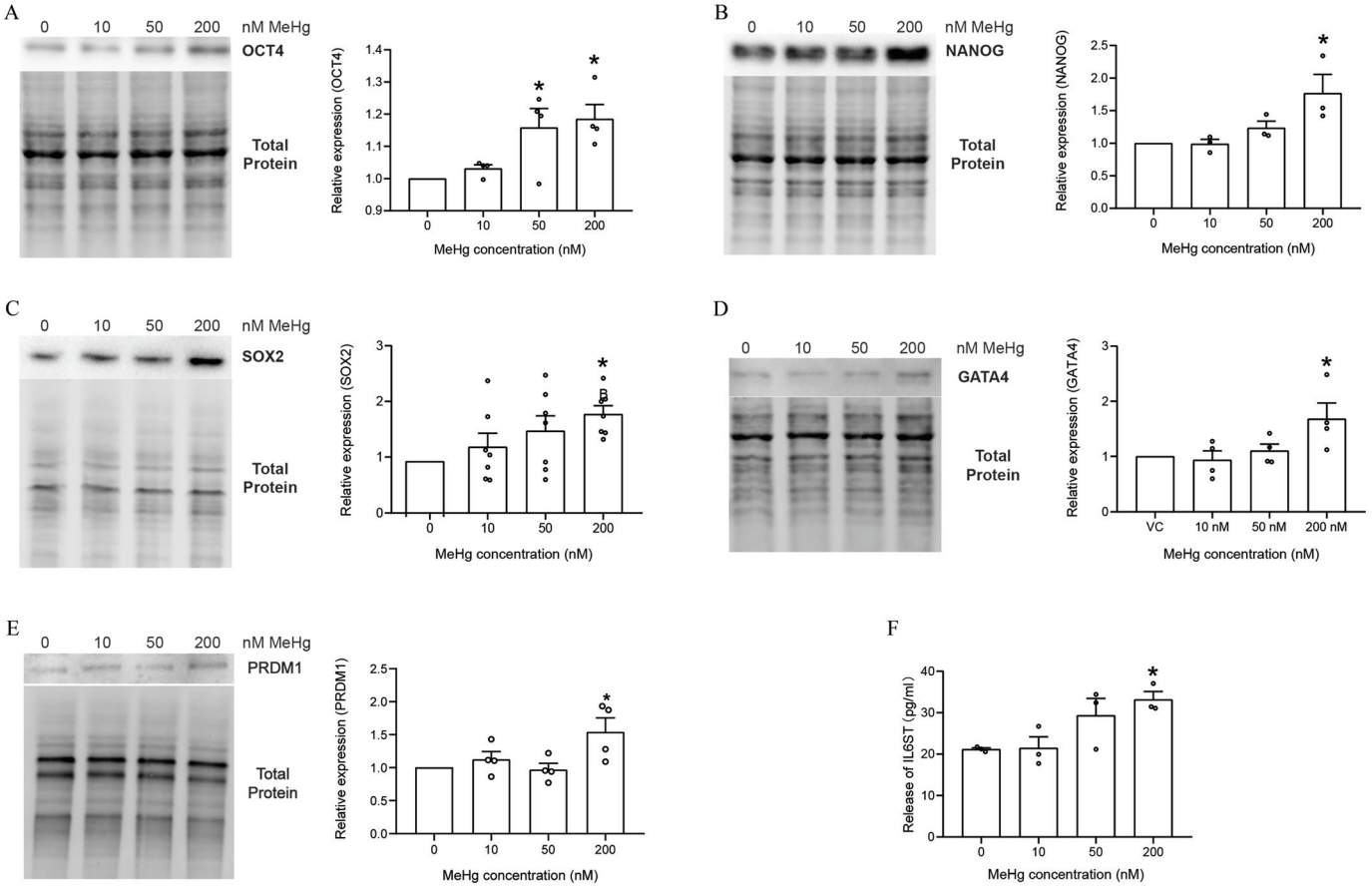

Figure 10. Expressions of selected cell lineage marker proteins, (A) OCT4, (B) NANOG, (C) SOX2, (D) GATA4, and (E) PRDM1 as measured using western blots, and (F) IL6ST as measured using ELISAs in hESCs after 6 d of exposure to 0, 10, 50, 200 nM MeHg. Data are presented as means ± SEMs with $N = 3$ for NANOG and IL6ST; $N = 4$ for OCT4, GATA4, and PRDM1; and $N = 7$ for SOX2. For western blots, each batch was first normalized to its sodium carbonate vehicle control (0 nM) before comparison. Thus, there are no error bars in the 0 nM MeHg groups for (A–E). The small circle symbols represent individual values of each experiment. One-way ANOVA was used at each time point to compare between the different doses, and the dose response of the treatment effects was significant. Dunnett's post hoc test was then used to compare the treatments to the vehicle control. Significance (*) was set at $p < 0.05$. The corresponding numeric data are provided in Table S8. Note: ANOVA, analysis of variance; ELISA, enzyme-linked immunosorbent assay; GATA4, GATA binding protein 4; hESC, human embryonic stem cell; IL6ST, interleukin 6 cytokine family signal transducer; MeHg, methylmercury; NANOG, Nanog homeobox; OCT4, octamer-binding transcription factor 4 [also known as POU5F1 (POU domain, class 5, transcription factor 1)]; PRDM1, PR domain-containing protein 1; SEM, standard error of the mean; SOX2, SRY-box transcription factor 2.

of early developmental disorders *in vivo*. This enhanced expression of self-renewal genes could be a result of the selection of a population of pluripotent cells for their ability to survive the MeHg ROS damage because of the higher level of oxidative capabilities. Increased ROS has been shown to prime stem cells for differentiation under intermediate levels (Bigarella et al. 2014). Therefore, hESCs with lower oxidative capabilities would begin to differentiate and become more prone to oxidative damage (Guo et al. 2010), resulting in death under prolonged MeHg exposure. The remaining cells would then be those that were not primed to differentiate and thus show higher levels of self-renewal gene expression.

It is known that the well-being of early embryo development in the oviduct and uterus is critical for successful implantation and a positive pregnancy outcome but that ~70% of human implantation sites are defective and, thus, prone to resorption (Hertig 1958). Spontaneous resorption is a major problem in assisted reproduction in humans (Drews et al. 2020). Findings from the present study suggest that exposure of blastocysts to nanomolar concentrations (10–200 nM) of MeHg, if it occurs *in vivo*, could disrupt early embryo development, implantation, and postimplantation development: outcomes that could explain the positive association between urinary mercury concentrations, oxidative stress, and spontaneous abortion observed in pregnant dental staff in Egypt (El-Badry et al. 2018). Monitoring blood and hair mercury concentrations during the preconception period to minimize the risk of adverse pregnancy outcomes has been practiced in the Hospital for Sick Children in Toronto, Canada (Neuman et al. 2014).

hESC-H9, the cell line used in the present study, can maintain a normal XX karyotype for >6 months in continuous culture, as described by Thomson et al. (1998). However, all findings in the present study were obtained from only one hESC line that was derived from an embryo of one donor. Therefore, the characteristics of this cell line may represent only the population that the donor represents. Other hESCs with different genetic and gender backgrounds should be tested for the effects of MeHg. A caution on the interpretation of the cell viability result is that the WST assay measured the activities of mitochondrial dehydrogenase as indicators for cell viability and cell proliferation. Given that we could not exclude the possibility that MeHg dosing can affect the protein levels or activities of mitochondrial dehydrogenase, the WST values may reflect the combined effects of MeHg on cell viability, cell proliferation, and mitochondrial dehydrogenase. In addition, even though a significant dose–response relationship between MeHg treatments and many measured end points was observed, the significant changes were mostly found in

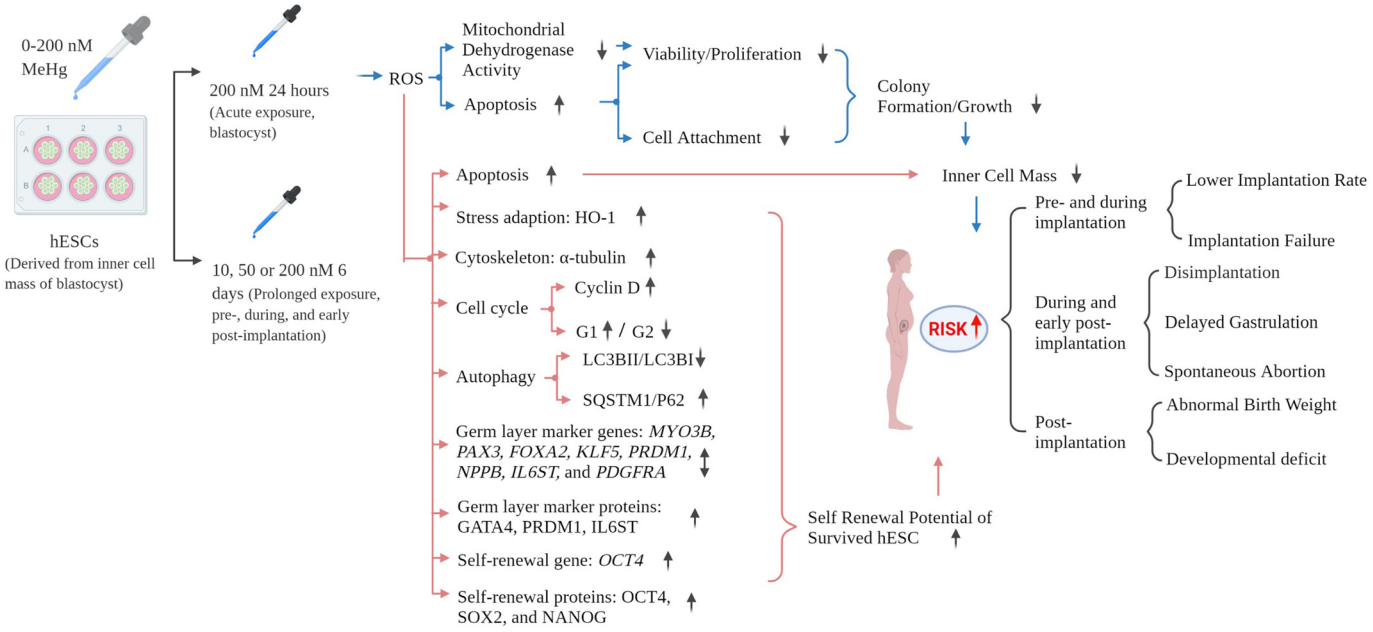

Figure 11. A schematic summary of the present study. Note: *FOXA2*, forkhead box A2; GATA4, GATA binding protein 4; hESC, human embryonic stem cell; HO-1, hemeoxygenase-1; IL6ST, interleukin 6 cytokine family signal transducer; *KLF5*, Kruppel-like factor 5; LC3B, microtubule-associated proteins 1A/1B light chain 3B; *MYO3B*, myosin IIIB; NANOG, Nanog homeobox; *NPPB*, natriuretic peptide B; OCT4, octamer-binding transcription factor 4 [also known as POU5F1 (POU domain, class 5, transcription factor 1)]; *PAX3*, paired box 3; *PDGFRA*, platelet-derived growth factor receptor-alpha; PRDM1, PR domain-containing protein 1; ROS, reactive oxygen species; SOX2, SRY-box transcription factor 2.

the 200 nM MeHg-treatment group, which was also associated with lower cell viability and higher stress after continuous dosing. Due to technical difficulties, we could not use the same method to assess apoptosis at different exposure times. New methodologies for measuring apoptosis in various stages of hESCs need to be established and applied in future studies.

In summary, our study confirmed that the reported cytotoxic effects of MeHg previously observed in fetal brain cells could also occur in undifferentiated hESC at similar or even lower concentrations (Figure 11). Our results suggest that the use of undifferentiated hESC shows merit for further validation as an *in vitro* model to screen chemicals for early developmental toxicities. Findings from the present study provide *in vitro* evidence that nanomolar concentrations of MeHg adversely affect the growth and health of hESCs, which suggests that *in vivo* exposure to MeHg can potentially result in adverse pregnancy and developmental outcomes, including implantation failure, spontaneous abortion, and developmental deficit.

Despite the risk of MeHg exposure, fish is an important source of nutrients beneficial to cardiovascular and neurological development (Mahaffey et al. 2011). With embryos and fetuses as the most sensitive stages of human development, it has become a delicate issue to balance the risks and benefits of fish consumption. Findings from the present study enrich the understanding of the potential pregnant and developmental outcomes associated with MeHg exposure and thus help vulnerable populations to minimize the risk of MeHg exposure through fish consumption.

Acknowledgments

We thank Y. Pan for reading through the manuscript and providing comments. We also thank the two editors and four reviewers for their positive comments and constructive suggestions that have significantly improved the manuscript from the initial submission. We are also thankful to A. Stalker, Regulatory Research Division, Center for Biologics Evaluation, Biologic and Radiopharmaceutical Drugs Directorate, Health Products and Food Branch, Health Canada for technical support in flow cytometry and E. Yumvihoze, Department of Biology, University of Ottawa, for technical support in MeHg concentration measurements. The present study was supported by an internal project funding provided to X. Jin in the Bureau of Chemical Safety, Food Directorate, Health Products and Food Branch, Health Canada, and a Discovery Grant from the Natural Sciences and Engineering Research Council of Canada and a Canada Research Chair to H.M. Chan.

References

Ajsuvakova OP, Tinkov AA, Aschner M, Rocha JBT, Michalke B, Skalnaya MG, et al. 2020. Sulfhydryl groups as targets of mercury toxicity. Coord Chem Rev 417:213343, PMID: 32905350, https://doi.org/10.1016/j.ccr.2020.213343.

Bigarella CL, Liang R, Ghaffari S. 2014. Stem cells and the impact of ROS signaling. Development 141(22):4206–4218, PMID: 25371358, https://doi.org/10.1242/dev.107086.

Burke K, Cheng Y, Li B, Petrov A, Joshi P, Berman RF, et al. 2006. Methylmercury elicits rapid inhibition of cell proliferation in the developing brain and decreases cell cycle regulator, cyclin E. Neurotoxicology 27(6):970–981, PMID: 17056119, https://doi.org/10.1016/j.neuro.2006.09.001.

Canuel R, de Grosbois SB, Atikessé L, Lucotte M, Arp P, Ritchie C, et al. 2006. New evidence on variations of human body burden of methylmercury from fish consumption. Environ Health Perspect 114(2):302–306, PMID: 16451872, https://doi.org/10.1289/ehp.7857.

Card DAG, Hebbar PB, Li L, Trotter KW, Komatsu Y, Mishina Y, et al. 2008. Oct4/Sox2-regulated miR-302 targets cyclin D1 in human embryonic stem cells. Mol Cell Biol 28(20):6426–6438, PMID: 18710938, https://doi.org/10.1128/MCB.00359-08.

Ceccatelli S, Daré E, Moors M. 2010. Methylmercury-induced neurotoxicity and apoptosis. Chem Biol Interact 188(2):301–308, PMID: 20399200, https://doi.org/10.1016/j.cbi.2010.04.007.

Chan HM, Receveur O. 2000. Mercury in the traditional diet of indigenous peoples in Canada. Environ Pollut 110(1):1–2, PMID: 15092850, https://doi.org/10.1016/S0269-7491(00)00061-0.

Choi AL, Mogensen UB, Bjerve KS, Debes F, Weihe P, Grandjean P, et al. 2014. Negative confounding by essential fatty acids in methylmercury neurotoxicity associations. Neurotoxicol Teratol 42:85–92, PMID: 24561639, https://doi.org/10.1016/j.ntt.2014.02.003.

Coleman ML, Olson MF. 2002. Rho GTPase signalling pathways in the morphological changes associated with apoptosis. Cell Death Differ 9(5):493–504, PMID: 11973608, https://doi.org/10.1038/sj.cdd.4400987.

Debes F, Budtz-Jørgensen E, Weihe P, White RF, Grandjean P. 2006. Impact of prenatal methylmercury exposure on neurobehavioral function at age 14 years. Neurotoxicol Teratol 28(5):536–547, PMID: 17067778, https://doi.org/10.1016/j.ntt.2006.02.005.

Debes F, Weihe P, Grandjean P. 2016. Cognitive deficits at age 22 years associated with prenatal exposure to methylmercury. Cortex 74:358–369, PMID: 26109549, https://doi.org/10.1016/j.cortex.2015.05.017.

dos Santos AA, Hort MA, Culbreth M, López-Granero C, Farina M, Rocha JB, et al. 2016. Methylmercury and brain development: a review of recent literature. J Trace Elem Med Biol 38:99–107, PMID: 26987277, https://doi.org/10.1016/j.jtemb.2016.03.001.

Drews B, Landaverde LF, Kühl A, Drews U. 2020. Spontaneous embryo resorption in the mouse is triggered by embryonic apoptosis followed by rapid removal via maternal sterile purulent inflammation. BMC Dev Biol 20(1):1, PMID: 31918653, https://doi.org/10.1186/s12861-019-0201-0.

Driscoll CT, Mason RP, Chan HM, Jacob DJ, Pirrone N. 2013. Mercury as a global pollutant: sources, pathways, and effects. Environ Sci Technol 47(10):4967–4983, PMID: 23590191, https://doi.org/10.1021/es305071v.

Dumitru R, Gama V, Fagan BM, Bower JJ, Swahari V, Pevny LH, et al. 2012. Human embryonic stem cells have constitutively active Bax at the Golgi and are primed to undergo rapid apoptosis. Mol Cell 46(5):573–583, PMID: 22560721, https://doi.org/10.1016/j.molcel.2012.04.002.

Edoff K, Raciti M, Moors M, Sundström E, Ceccatelli S. 2017. Gestational age and sex influence the susceptibility of human neural progenitor cells to low levels of MeHg. Neurotox Res 32(4):683–693, PMID: 28756503, https://doi.org/10.1007/s12640-017-9786-x.

El Asar HM, Mohammed EA, Aboulhoda BE, Emam HY, Imam AA-A. 2019. Selenium protection against mercury neurotoxicity: modulation of apoptosis and autophagy in the anterior pituitary. Life Sci 231:116578, PMID: 31211996, https://doi.org/10.1016/j.lfs.2019.116578.

El-Badry A, Rezk M, El-Sayed H. 2018. Mercury-induced oxidative stress may adversely affect pregnancy outcome among dental staff: a cohort study. Int J Occup Environ Med 9(3):113–119, PMID: 29995016, https://doi.org/10.15171/ijoem.2018.1181.

Fang F, Angulo B, Xia N, Sukhwani M, Wang Z, Carey CC, et al. 2018. A PAX5–OCT4–PRDM1 developmental switch specifies human primordial germ cells. Nat Cell Biol 20(6):655–665, PMID: 29713018, https://doi.org/10.1038/s41556-018-0094-3.

Farina M, Aschner M. 2017. Methylmercury-induced neurotoxicity: focus on pro-oxidative events and related consequences. In: *Neurotoxicity of Metals. Advances in Neurobiology*, vol 18. Aschner M, Costa L, eds. Cham, Switzerland: Springer, 267–286.

Gatti R, Belletti S, Uggeri J, Vettori MV, Mutti A, Scandroglio R, et al. 2004. Methylmercury cytotoxicity in PC12 cells is mediated by primary glutathione depletion independent of excess reactive oxygen species generation. Toxicology 204(2–3):175–185, PMID: 15388243, https://doi.org/10.1016/j.tox.2004.06.023.

Grandjean P, Herz KT. 2011. Methylmercury and brain development: imprecision and underestimation of developmental neurotoxicity in humans. Mt Sinai J Med 78(1):107–118, PMID: 21259267, https://doi.org/10.1002/msj.20228.

Grandjean P, Weihe P, White RF, Debes F, Araki S, Yokoyama K, et al. 1997. Cognitive deficit in 7-year-old children with prenatal exposure to methylmercury. Neurotoxicol Teratol 19(6):417–428, PMID: 9392777, https://doi.org/10.1016/S0892-0362(97)00097-4.

Guo Y-L, Chakraborty S, Rajan SS, Wang R, Huang F. 2010. Effects of oxidative stress on mouse embryonic stem cell proliferation, apoptosis, senescence, and self-renewal. Stem Cells Dev 19(9):1321–1331, PMID: 20092403, https://doi.org/10.1089/scd.2009.0313.

Ha E, Basu N, Bose-O'Reilly S, Dórea JG, McSorley E, Sakamoto M, et al. 2017. Current progress on understanding the impact of mercury on human health. Environ Res 152:419–433, PMID: 27444821, https://doi.org/10.1016/j.envres.2016.06.042.

Hanson MA, Skinner MK. 2016. Developmental origins of epigenetic transgenerational inheritance. Environ Epigenet 2(1):dvw002, PMID: 27390622, https://doi.org/10.1093/eep/dvw002.

Hartig SM. 2013. Basic image analysis and manipulation in ImageJ. Curr Protoc Mol Biol Chapter 14:Unit14.15, PMID: 23547012, https://doi.org/10.1002/0471142727.mb1415s102.

Heindel JJ. 2019. The developmental basis of disease: update on environmental exposures and animal models. Basic Clin Pharmacol Toxicol 125(suppl 3):5–13, PMID: 30265444, https://doi.org/10.1111/bcpt.13118.

Hertig AT. 1958. The evolution of a research program. Am J Obstet Gynecol 76(2):252–270, PMID: 13559314, https://doi.org/10.1016/0002-9378(58)90212-6.

Hu G, Kim J, Xu Q, Leng Y, Orkin SH, Elledge SJ. 2009. A genome-wide RNAi screen identifies a new transcriptional module required for self-renewal. Genes Dev 23(7):837–848, PMID: 19339689, https://doi.org/10.1101/gad.1769609.

Huppertz B, Herrler A. 2005. Regulation of proliferation and apoptosis during development of the preimplantation embryo and the placenta. Birth Defects Res C Embryo Today 75(4):249–261, PMID: 16425254, https://doi.org/10.1002/bdrc.20056.

Jayashankar S, Glover CN, Folven KI, Brattelid T, Hogstrand C, Lundebye A-K. 2011. Cerebral gene expression in response to single or combined gestational exposure to methylmercury and selenium through the maternal diet. Cell Biol Toxicol 27(3):181–197, PMID: 21240674, https://doi.org/10.1007/s10565-010-9180-4.

Julvez J, Debes F, Weihe P, Choi A, Grandjean P. 2010. Sensitivity of continuous performance test (CPT) at age 14 years to developmental methylmercury exposure. Neurotoxicol Teratol 32(6):627–632, PMID: 20699117, https://doi.org/10.1016/j.ntt.2010.08.001.

Kajiwara Y, Inouye M. 1986. Effects of methylmercury and mercuric chloride on preimplantation mouse embryos in vivo. Teratology 33(2):231–237, PMID: 3738818, https://doi.org/10.1002/tera.1420330210.

Kang C, Xu Q, Martin TD, Li MZ, Demaria M, Aron L, et al. 2015. The DNA damage response induces inflammation and senescence by inhibiting autophagy of GATA4. Science 349(6255):aaa5612, PMID: 26404840, https://doi.org/10.1126/science.aaa5612.

Karagas MR, Choi AL, Oken E, Horvat M, Schoeny R, Kamai E, et al. 2012. Evidence on the human health effects of low-level methylmercury exposure. Environ Health Perspect 120(6):799–806, PMID: 22275730, https://doi.org/10.1289/ehp.1104494.

Kerper LE, Ballatori N, Clarkson TW. 1992. Methylmercury transport across the blood-brain barrier by an amino acid carrier. Am J Physiol 262(5 pt 2):R761–R765, PMID: 1590471, https://doi.org/10.1152/ajpregu.1992.262.5.R761.

Konstantinidou A, Givalos N, Gakiopoulou H, Korkolopoulou P, Kotsiakis X, Boviatsis E, et al. 2007. Caspase-3 immunohistochemical expression is a marker of apoptosis, increased grade and early recurrence in intracranial meningiomas. Apoptosis 12(4):695–705, PMID: 17143787, https://doi.org/10.1007/s10495-006-0001-4.

Lenton EA, Neal LM, Sulaiman R. 1982. Plasma concentrations of human chorionic gonadotropin from the time of implantation until the second week of pregnancy. Fertil Steril 37(6):773–778, PMID: 7115557, https://doi.org/10.1016/s0015-0282(16)46337-5.

Li C, He B, Huang C, Yang H, Cao L, Huang J, et al. 2017. Sex-determining region Y-box 2 promotes growth of lung squamous cell carcinoma and directly targets cyclin D1. DNA Cell Biol 36(4):264–272, PMID: 28151013, https://doi.org/10.1089/dna.2016.3562.

Li J, Fu KZ, Vemula S, Le XC, Li X-F. 2015. Studying developmental neurotoxic effects of bisphenol A (BPA) using embryonic stem cells. J Environ Sci (China) 36:173–177, PMID: 26456619, https://doi.org/10.1016/j.jes.2015.08.002.

Lopata A. 1996. Implantation of the human embryo. Hum Reprod 11(suppl 1):175–184, PMID: 8968778, https://doi.org/10.1093/humrep/11.suppl_5.175.

Mahaffey KR, Sunderland EM, Chan HM, Choi AL, Grandjean P, Mariën K, et al. 2011. Balancing the benefits of n-3 polyunsaturated fatty acids and the risks of methylmercury exposure from fish consumption. Nutr Rev 69(9):493–508, PMID: 21884130, https://doi.org/10.1111/j.1753-4887.2011.00415.x.

Mori N, Yasutake A, Marumoto M, Hirayama K. 2011. Methylmercury inhibits electron transport chain activity and induces cytochrome *c* release in cerebellum mitochondria. J Toxicol Sci 36(3):253–259, PMID: 21628953, https://doi.org/10.2131/jts.36.253.

Neuman G, Gareri J, Koren G. 2014. Preconceptional monitoring of mercury levels in hair and blood as a tool for minimizing associated reproductive risks. Ther Drug Monit 36(6):696–698, PMID: 24831651, https://doi.org/10.1097/FTD.0000000000000096.

Oken E, Wright RO, Kleinman KP, Bellinger D, Amarasiriwardena CJ, Hu H, et al. 2005. Maternal fish consumption, hair mercury, and infant cognition in a U.S. cohort. Environ Health Perspect 113(10):1376–1380, PMID: 16203250, https://doi.org/10.1289/ehp.8041.

Pampfer S, Donnay I. 1999. Apoptosis at the time of embryo implantation in mouse and rat. Cell Death Differ 6(6):533–545, PMID: 10381643, https://doi.org/10.1038/sj.cdd.4400516.

Pauklin S, Madrigal P, Bertero A, Vallier L. 2016. Initiation of stem cell differentiation involves cell cycle-dependent regulation of developmental genes by cyclin D. Genes Dev 30(4):421–433, PMID: 26883361, https://doi.org/10.1101/gad.271452.115.

Pauklin S, Vallier L. 2013. The cell-cycle state of stem cells determines cell fate propensity. Cell 155(1):135–147, PMID: 24074866, https://doi.org/10.1016/j.cell.2013.08.031.

Pauklin S, Vallier L. 2015. Activin/Nodal signalling in stem cells. Development 142(4):607–619, PMID: 25670788, https://doi.org/10.1242/dev.091769.

Prpić I, Milardović A, Vlašić-Cicvarić I, Špiric Z, Nišević JR, Vukelić P, et al. 2017. Prenatal exposure to low-level methylmercury alters the child's fine motor skills at the age of 18 months. Environ Res 152:369–374, PMID: 27771004, https://doi.org/10.1016/j.envres.2016.10.011.

Rodolfo C, Di Bartolomeo S, Cecconi F. 2016. Autophagy in stem and progenitor cells. Cell Mol Life Sci 73(3):475–496, PMID: 26502349, https://doi.org/10.1007/s00018-015-2071-3.

Rusten TE, Stenmark H. 2010. p62, an autophagy hero or culprit? Nat Cell Biol 12(3):207–209, PMID: 20190829, https://doi.org/10.1038/ncb0310-207.

Saunders A, Faiola F, Wang J. 2013. Concise review: pursuing self-renewal and pluripotency with the stem cell factor Nanog. Stem Cells 31(7):1227–1236, PMID: 23653415, https://doi.org/10.1002/stem.1384.

Shao Y, Figeys D, Ning Z, Mailloux R, Chan HM. 2015. Methylmercury can induce Parkinson's-like neurotoxicity similar to 1-methyl-4-phenylpyridinium: a genomic and proteomic analysis on MN9D dopaminergic neuron cells. J Toxicol Sci 40(6):817–828, PMID: 26558463, https://doi.org/10.2131/jts.40.817.

She S, Wei Q, Kang B, Wang Y-J. 2017. Cell cycle and pluripotency: convergence on octamer-binding transcription factor 4 (review). Mol Med Rep 16(5):6459–6466, PMID: 28901500, https://doi.org/10.3892/mmr.2017.7489.

Sheehan MC, Burke TA, Navas-Acien A, Breysse PN, McGready J, Fox MA. 2014. Global methylmercury exposure from seafood consumption and risk of developmental neurotoxicity: a systematic review. Bull World Health Organ 92(4):254–269F, PMID: 24700993, https://doi.org/10.2471/BLT.12.116152.

Spindle A, Matsumoto N. 1987. Enhancement of methylmercury toxicity by L-cystine in cultured mouse blastocysts. Reprod Toxicol 1(4):279–284, PMID: 2980393, https://doi.org/10.1016/0890-6238(87)90019-0.

Stummann TC, Hareng L, Bremer S. 2009. Hazard assessment of methylmercury toxicity to neuronal induction in embryogenesis using human embryonic stem cells. Toxicology 257(3):117–126, PMID: 19150642, https://doi.org/10.1016/j.tox.2008.12.018.

Tamm C, Duckworth J, Hermanson O, Ceccatelli S. 2006. High susceptibility of neural stem cells to methylmercury toxicity: effects on cell survival and neuronal differentiation. J Neurochem 97(1):69–78, PMID: 16524380, https://doi.org/10.1111/j.1471-4159.2006.03718.x.

Thomson JA, Itskovitz-Eldor J, Shapiro SS, Waknitz MA, Swiergiel JJ, Marshall VS, et al. 1998. Embryonic stem cell lines derived from human blastocysts. Science 282(5391):1145–1147, PMID: 9804556, https://doi.org/10.1126/science.282.5391.1145.

Tra T, Gong L, Kao L-P, Li X-L, Grandela C, Devenish RJ, et al. 2011. Autophagy in human embryonic stem cells. PLoS One 6(11):e27485, PMID: 22110659, https://doi.org/10.1371/journal.pone.0027485.

Varum S, Momčilović O, Castro C, Ben-Yehudah A, Ramalho-Santos J, Navara CS. 2009. Enhancement of human embryonic stem cell pluripotency through inhibition of the mitochondrial respiratory chain. Stem Cell Res 3(2–3):142–156, PMID: 19716358, https://doi.org/10.1016/j.scr.2009.07.002.

Wang X, Yan M, Zhao L, Wu Q, Wu C, Chang X, et al. 2016. Low-dose methylmercury-induced apoptosis and mitochondrial DNA mutation in human embryonic neural progenitor cells. Oxid Med Cell Longev 2016:5137042, PMID: 27525052, https://doi.org/10.1155/2016/5137042.

Wang Y, Zhang H. 2019. Regulation of autophagy by mTOR signaling pathway. Adv Exp Med Biol 1206:67–83, PMID: 31776980, https://doi.org/10.1007/978-981-15-0602-4_3.

Watanabe J, Nakamachi T, Ohtaki H, Naganuma A, Shioda S, Nakajo S. 2013. Low dose of methylmercury (MeHg) exposure induces caspase mediated-apoptosis in cultured neural progenitor cells. J Toxicol Sci 38(6):931–935, PMID: 24213013, https://doi.org/10.2131/jts.38.931.

Worley JR, Parker GC. 2019. Effects of environmental stressors on stem cells. World J Stem Cells 11(9):565–577, PMID: 31616535, https://doi.org/10.4252/wjsc.v11.i9.565.

Xu M, Yan C, Tian Y, Yuan X, Shen X. 2010. Effects of low level of methylmercury on proliferation of cortical progenitor cells. Brain Res 1359:272–280, PMID: 20813099, https://doi.org/10.1016/j.brainres.2010.08.069.

Xu Y, Zhang Y, García-Cañaveras JC, Guo L, Kan M, Yu S, et al. 2020. Chaperone-mediated autophagy regulates the pluripotency of embryonic stem cells. Science 369(6502):397–403, PMID: 32703873, https://doi.org/10.1126/science.abb4467.

Yuan JS, Reed A, Chen F, Stewart CN Jr. 2006. Statistical analysis of real-time PCR data. BMC Bioinformatics 7:85, PMID: 16504059, https://doi.org/10.1186/1471-2105-7-85.

Yuntao F, Chenjia G, Panpan Z, Wenjun Z, Suhua W, Guangwei X, et al. 2016. Role of autophagy in methylmercury-induced neurotoxicity in rat primary astrocytes. Arch Toxicol 90(2):333–345, PMID: 25488884, https://doi.org/10.1007/s00204-014-1425-1.

Zhao A, Yang L, Ma K, Sun M, Li L, Huang J, et al. 2016. Overexpression of cyclin D1 induces the reprogramming of differentiated epidermal cells into stem cell-like cells. Cell Cycle 15(5):644–653, PMID: 26890246, https://doi.org/10.1080/15384101.2016.1146838.

Zhou J, Su P, Wang L, Chen J, Zimmermann M, Genbacev O, et al. 2009. mTOR supports long-term self-renewal and suppresses mesoderm and endoderm activities of human embryonic stem cells. Proc Natl Acad Sci USA 106(19):7840–7845, PMID: 19416884, https://doi.org/10.1073/pnas.0901854106.